

Magmatic Activity on a Motionless Plate: the Case of East Island, Crozet Archipelago (Indian Ocean)

Christine Marie Meyzen^{1*}, Andrea Marzoli^{1,2}, Giuliano Bellieni¹ and Gilles Levrès³

¹Dipartimento di Geoscienze, Università degli Studi di Padova, Via G. Gradenigo, 6, 35131 Padova, Italy; ²IGG-CNR Padova, Università degli Studi di Padova, Via G. Gradenigo, 6, 35131 Padova, Italy; ³Geofluidos, Centro de Geociencias, Universidad Nacional Autónoma de México, Blvd. Juriquilla No. 3001, 76230 Querétaro, Mexico

*Corresponding author. E-mail: christine.meyzen@unipd.it

Received July 10, 2015; Accepted July 7, 2016

ABSTRACT

Lying atop the relatively motionless Antarctic plate (velocity $\sim 6.46 \text{ mm a}^{-1}$), the Crozet archipelago, midway between Madagascar and Antarctica, is a region of unusually shallow (1543–1756 m) and thickened oceanic crust (10–16.5 km), high geoid height, and deep low-velocity zone, which may represent the surface expression of a mantle plume. Here, new major and trace element data are presented for Quaternary alkali basalts of the subaerial eruptive stage of East Island, the most easterly and oldest island ($\sim 9 \text{ Ma}$) of the Crozet archipelago. Crystallization at uppermost mantle depths and phenocryst accumulation have strongly affected the parental magma compositions. Trace element patterns show a large negative K anomaly relative to Ta–La, moderate depletions in Rb and Ba with respect to Th–U, and heavy rare earth element depletions relative to light rare earth elements. These characteristics allow limits to be placed upon the composition and mineralogy of the mantle source of the magmas. The average trace element pattern of the East Island basalts can be matched by $\sim 1.7\%$ melting of a garnet–phlogopite-bearing peridotite source. The stability field of phlogopite restricts melting depths to lithospheric levels. The modelled source composition requires a multistage evolution in which the mantle has been depleted by melt extraction before being metasomatized by alkali-rich plume-derived melts. The depleted mantle component is inferred to be sourced from residual mantle plume remnants that stagnated at the melting locus owing to a weak lateral flow velocity inside the melting region, whose accumulation progressively forms a depleted lithospheric root above the plume core. Low-degree, alkali-rich melts are probably derived from the plume source. Such a mantle source evolution may be general to both terrestrial and extraterrestrial environments in which the lateral component velocity of the mantle flow field is extremely slow.

Key words: Crozet plume; lithosphere; Indian Ocean; magmatism; Antarctic plate; lithospheric root

INTRODUCTION

In contrast to the large number of geochemical studies carried out on the Kerguelen and Mascarene archipelagos in the Indian Ocean, the magmatic evolution of the Crozet Islands has received far less attention (Gunn *et al.*, 1970; Zhou, 1996; Breton *et al.*, 2013). The Crozet archipelago comprises a number of islands and islets (Figs 1 and 2a), divided into two groups: an older eastern island

group ($< 9 \text{ Ma}$) composed of large-scale volcanic landmasses (East and Possession islands), and a younger western group ($< 5.5 \text{ Ma}$) composed of two small islands (Pig and Penguin) and islets (Apostle Islets). A detailed description of the regional geodynamic context is given in [Supplementary Data Electronic Appendix 1](#) (supplementary data are available for downloading at <http://www.petrology.oxfordjournals.org>). Magmatic

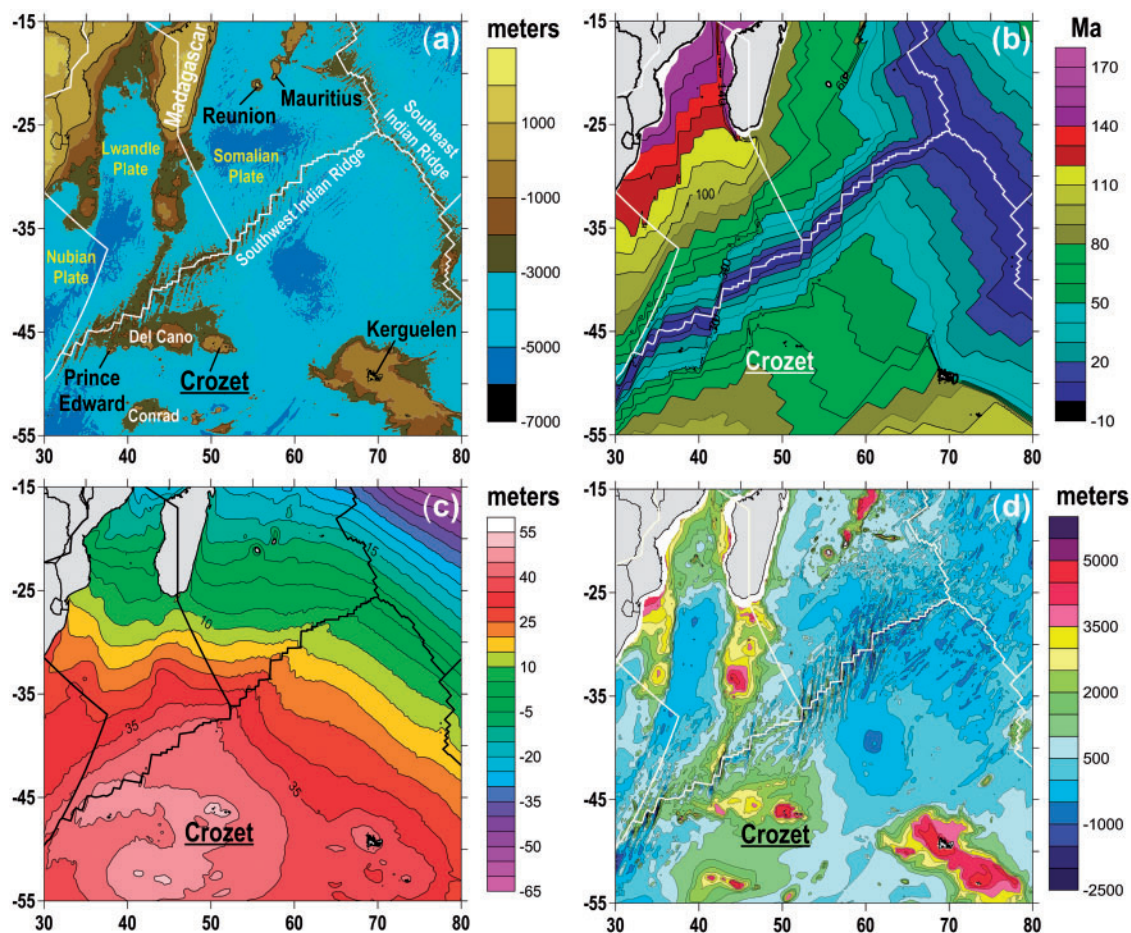


Fig. 1. Maps of the southwestern Indian Ocean. (a) Topographic map of continents and ocean floor (Becker *et al.*, 2009). (b) Age distribution (Ma) of the Indian Ocean seafloor (Müller *et al.*, 2008). (c) Geoid height (m) (Sandwell & McAdoo, 1990). (d) Residual depth (m) of the oceanic basement (Crosby *et al.*, 2006). Plate boundaries are from Argus *et al.* (2011) and DeMetz *et al.* (1990). All data have been retrieved from the GeoMapApp application (www.geomapp.org).

processes occurring in this archipelago probably represent an end-member case for models of intraplate magmatism because of its location on the slowest moving plate on Earth, the Antarctic plate ($\sim 6.46 \text{ mm a}^{-1}$; King & Adam, 2014), and an associated upwelling buoyancy flux estimated at $0.25\text{--}0.5 \text{ Mg s}^{-1}$ (e.g. Sleep, 1990; King & Adam, 2014), placing it among the weakest mantle upwellings on Earth. The mantle upwelling and, therefore, melting rates beneath the Crozet Islands are estimated to be among the lowest of all Earth's upwellings and have been strongly spatially focused for the last ~ 10 Myr. This is probably the reason why the Crozet Bank is one of the shallowest of all oceanic island swells, with a height of 1543–1756 m (Monnereau & Cazenave, 1990; Sleep, 1990; King & Adam, 2014), and why measurements of heat flux yield the highest value (96 mW m^{-2} ; Courtney & Recq, 1986) so far observed among ocean islands (Harris & McNutt, 2007). This prolonged focusing of the melting activity is predicted to induce long-term interactions of the upwelling mantle with the overlying Antarctic lithosphere. The area is also associated with a regional geoid high (Monnereau & Cazenave, 1990) and a deep low-velocity zone (down to 2350 km; Montelli *et al.*, 2004,

2006). All these features point towards the presence of a significant mantle thermal anomaly below the archipelago. However, for decades, scientists have been puzzled by the proposed existence of a mantle plume fuelling the volcanism of the Crozet Islands, because of the absence of a preserved prominent volcanic record on the adjacent African, Antarctic and Australian plates that could link the present-day Crozet archipelago to a precursor flood basalt province.

Here we focus on the Quaternary volcanic rocks of the easternmost and oldest island of the Crozet archipelago, East Island (Fig. 2a), to examine the effects of a near-stationary plate on intraplate melting processes. East Island ($\sim 130 \text{ km}^2$) forms a central volcanic cone incised by deep valleys radiating from its center (Mt Dusclèmeur), separated by steep-sided ridges (Fig. 2b; see Supplementary Data Electronic Appendix 1 for a detailed description of East Island geology). This glacially eroded volcanic peak rises ~ 1000 m above sea level and was built *c.* 9 Myr ago (Gunn *et al.*, 1970; Lameyre & Nougier, 1982; Chevallier *et al.*, 1983). The island has not been visited since the late 1970s. Gunn *et al.* (1970) undertook preliminary field mapping associated with a

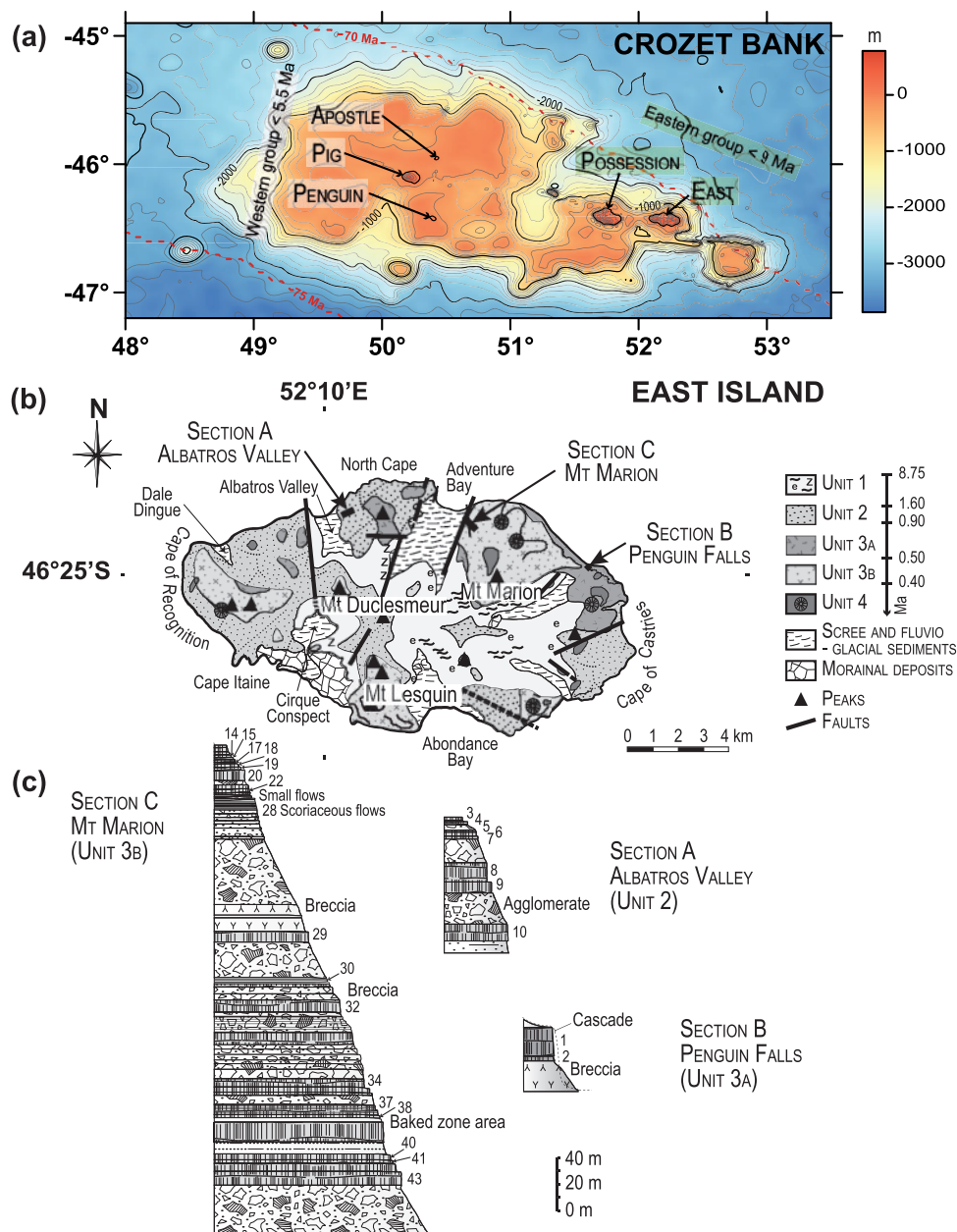


Fig. 2. Maps of the Crozet Bank and East Island and the studied lava sections. (a) Bathymetric map of the Crozet Bank from the Global Multi Resolution Topography data portal (www.marine-geo.org). Isobaths are labeled every 200 m. Red dashed lines indicate sea floor ages (Müller *et al.*, 2008). All data have been retrieved from GeoMapApp (www.geomapapp.org). (b) Schematic geological map of East Island [modified from Lameyre & Nougier (1982) and Verwoerd *et al.* (1990)] showing the location of the sampled sections. Unit 1: brecciated and metamorphosed dyke complex with layered plutonic rocks (~), epidote (e) and zeolite (z). Unit 2: conglomerates, agglomerates and thin basaltic flows. Unit 3A: volcanic agglomerates capped by hawaiite flows. Unit 3B: volcanic agglomerates and lava flows. Unit 4: scoriaceous cones. (c) Lava sections sampled by Gunn *et al.* (1970) [modified from Gunn *et al.* (1970) and Lameyre & Nougier (1982)]. Lava flows are numbered following Gunn *et al.* (1970). K–Ar age determinations for each unit are from Verwoerd *et al.* (1990).

petrological study of East Island lavas. Later, Lameyre & Nougier (1982) further detailed the island's geology. Four distinct volcanic cycles (first, 8.75–2.9 Ma; second, 1.6–0.9 Ma; third, 0.5–0.4 Ma; fourth, <0.1 Ma) were recognized based on K–Ar geochronology (Chevallier *et al.*, 1983; Verwoerd *et al.*, 1990). The lavas emitted during the second and third cycles define an alkaline suite (Gunn *et al.*, 1970). Gunn *et al.* (1970) suggested

that they were derived from a single alkaline parental magma by low-pressure fractionation. From the sparse geochemical data available for East Island, and the archipelago in general, it seems that most basalts are alkalic rather than tholeiitic (Gunn *et al.*, 1970; Zhou, 1996; Giret *et al.*, 2002; Breton *et al.*, 2013). The existing, albeit limited, Sr–Nd–Pb radiogenic isotope data for the rocks of East and Possession Islands, which constitute

the oldest parts of the archipelago (Fig. 2a), point to the presence of a remarkably homogeneous mantle source, similar to that of the Mascarene shield volcanoes (Mahoney *et al.*, 1996; Breton *et al.*, 2013). The youngest part of the archipelago (Pig and Penguin Islands and Apostle Islets, Fig. 2a) has a distinct Sr–Nd–Pb isotopic signature, requiring a large contribution from a FOZO-like mantle component to its mantle source (Breton *et al.*, 2013).

Understanding the petrogenesis of alkali basalts in the Crozet archipelago requires a comprehensive approach, including mineral chemistry and whole-rock major and trace element compositions, as presented here. Based on these data we discuss the importance of assimilation and fractional crystallization processes in determining the chemistry of East Island lavas. We conclude that the chemical characteristics of East Island lavas are the result of low extents of melting of residual metasomatized mantle remnants.

SAMPLING AND METHODS

Sample location and selection

A full description of the regional geodynamic context, as well as the geology and stratigraphy of East Island, is provided in [Supplementary Data Electronic Appendix 1](#). The samples from East Island analyzed here were cored in 1969, as reported by Gunn *et al.* (1970), from the northern part of the island along three stratigraphic sections (Fig. 2b and c): Albatros Valley (section A, Fig. 2b and c), Penguin Falls (section B, Fig. 2b and c), and Mt Marion (section C, Fig. 2b and c), corresponding to the second (Unit 2), lower third (Unit 3a) and upper third (Unit 3b) units of the stratigraphy, respectively. It should be noted that according to the latest geographical terminology the Abundance Bay and East Shipwreck Bay sections of Gunn *et al.* (1970) have been renamed as the Albatros Valley (section A) and Mount Marion sections (section C, Fig. 2b and c), respectively. Twenty-five samples were selected to ensure relatively uniform stratigraphic coverage of these three sections and were classified with respect to phenocryst abundance and assemblage, vesicularity, and extent of alteration. Petrographic and mineralogical descriptions are given in [Supplementary Data Electronic Appendix 1](#). Representative samples of each subtype were selected for geochemical analysis.

Rationale for the separation of groundmasses in East Island lavas

Because most of the samples are small (2.5 cm × 1.5 cm; see [Supplementary Data Electronic Appendix 1](#)), coarsely phytic core samples, we chose to carefully extract and analyze only their groundmasses. The rationale for implementing such a separation procedure was two-fold: (1) to overcome potential sample

heterogeneity; (2) to avoid accumulative crystal effects so as to obtain the most reliable residual melt composition.

Because of their variable phenocryst contents, as high as ~50%, and their small size ([Supplementary Data Electronic Appendix 1](#)), our samples are not representative of residual liquids. The accumulation of phenocrysts (olivine and clinopyroxene) strongly biases the bulk chemical compositions relative to those of melts, because (1) crystals may be xenocrysts inherited from either the mantle source or the oceanic crust, or a previous melting event, and (2) their modal distribution in the analyzed aliquot may strongly diverge from that of the host lava flow. The most reliable way to overcome these difficulties is to analyze the groundmass composition.

The validity of this approach was tested by least-squares mass-balance calculations to determine the proportions of crystals that must be added to the groundmass compositions to yield the whole-rock analyses, based on published whole-rock analyses by Gunn *et al.* (1970) and new major element analyses of the phenocrysts in the East Island lavas (see [Supplementary Data Electronic Appendices 2–5](#)). The results are shown in [Table 1](#). The proportions of olivine and clinopyroxene broadly correspond to the observed modal proportions, varying from ~9.3 to ~26.4%. The least-squares sum is well beyond the X-ray fluorescence (XRF) analytical errors for two of the samples, CE0061 AV and CE0054 AV. This could be ascribed to the lower precision of the Gunn *et al.* (1970) major oxide analyses compared with modern state-of-the-art data.

Whole-rock groundmass compositions

Single groundmass analyses from each section (A, B and C, Fig. 2c) sampled by Gunn *et al.* (1970) are presented in [Tables 2 and 3](#). Our major element data for aphyric or near-aphyric samples (e.g. CE0432 M,

Table 1. Least-squares mass-balance calculations

Sample	X_{OL}	X_{CPX}	X_{OP}	X_{PL}	X_{LQ}	R^2
CE0061 AV	0.072	0.102	—	0.064	0.761	0.948
CE0054 AV	0.025	0.223	0.032	—	0.72	0.831
CE0041 AV	0.018	0.113	0.006	—	0.863	0.066
CE0031 AV	0.035	0.229	0.002	—	0.734	0.011
CE0021 PF	0.064	0.029	0.004	—	0.903	0.057
CE0016 PF	0.075	0.047	0.018	—	0.86	0.095
CE0362 M	0.052	0.077	0.003	—	0.867	0.061
CE032 M	0.065	0.1	0.005	—	0.83	0.037
CE0303 M	0.099	0.059	—	0.019	0.823	0.018
CE0282 M	0.02	0.133	—	—	0.846	0.299
CE0151 M	0.102	0.051	0.002	—	0.845	0.026

Least-squares mass-balance calculations (Bryan *et al.*, 1969) demonstrate that [liquid composition (X_{LQ})] + [olivine (X_{OL}) + clinopyroxene (X_{CPX}) ± plagioclase (X_{PL}) ± oxides (X_{OP})] = [whole-rock composition]. Whole-rock compositions for these calculations are from Gunn *et al.* (1970) on the same samples. The calculations were made using SiO₂, TiO₂, Al₂O₃, FeO, MgO, CaO, Na₂O and K₂O, with all oxides weighted. R^2 is the sum of squares of residuals for those same oxides. AV, Albatros Valley; PF, Penguin Falls; M, Mt Marion.

Table 2. Major element data (in wt %) for lavas from East Island (Crozet archipelago, Indian Ocean); all samples are basalts in TAS classification

	SiO ₂	TiO ₂	Al ₂ O ₃	Fe ₂ O _{3t}	MnO	MgO	CaO	Na ₂ O	K ₂ O	P ₂ O ₅	LOI	H ₂ O ⁻	Total
<i>Albatros Valley, Unit 2</i>													
CE0106 AV	47.58	3.27	14.59	12.55	0.18	6.83	11.68	2.70	1.34	0.49	-0.57	0.12	100.76
CE0084 AV	47.00	3.18	12.93	11.05	0.15	9.90	12.73	2.19	1.09	0.41	-0.24	0.15	100.54
CE0061 AV	46.76	3.12	14.41	14.06	0.19	6.27	12.07	2.60	1.27	0.48	-0.58	0.12	100.77
CE0054 AV	46.45	3.07	14.33	13.88	0.19	6.36	12.14	2.54	1.21	0.46	-0.54	0.14	100.23
CE0041 AV	46.82	3.13	14.67	14.15	0.20	6.00	11.92	2.77	1.25	0.48	-0.65	0.09	100.83
CE0031 AV	46.59	3.03	14.25	13.94	0.20	6.57	12.08	2.56	1.17	0.46	-0.59	0.09	100.35
<i>Penguin Falls, Unit 3a</i>													
CE0021 PF	46.11	2.80	12.27	12.30	0.16	11.27	12.50	2.23	1.03	0.39	-0.46	0.11	100.71
CE0016 PF	46.27	2.85	12.23	11.89	0.16	10.85	12.87	2.19	0.97	0.39	-0.40	0.12	100.39
<i>Mt Marion, Unit 3b</i>													
CE0432 M	47.18	2.87	13.42	12.61	0.18	7.67	12.64	2.26	1.20	0.38	-0.39	0.14	100.16
CE0412 M	48.24	2.87	12.94	11.05	0.16	8.50	13.52	2.31	1.09	0.37	-0.50	0.08	100.63
CE0402 M	47.94	2.77	12.68	11.41	0.17	8.48	13.07	2.36	1.13	0.39	-0.37	0.12	100.15
CE0383 M	48.22	2.68	13.77	12.17	0.17	9.02	10.67	2.69	1.33	0.49	-0.58	0.08	100.71
CE0371 M	48.23	2.68	14.03	11.82	0.17	8.27	10.74	2.75	1.34	0.48	-0.58	0.09	100.02
CE0344 M	47.82	3.26	15.02	12.84	0.18	6.12	11.07	2.82	1.41	0.48	-0.62	0.08	100.48
CE032 M	47.73	2.86	14.05	12.26	0.17	8.66	11.38	2.45	1.05	0.42	-0.38	0.08	100.73
CE0303 M	47.27	3.01	13.52	12.06	0.17	8.27	11.93	2.48	1.30	0.42	-0.34	0.16	100.25
CE0293 M	47.36	2.91	13.90	12.65	0.17	8.97	11.57	2.42	1.17	0.41	-0.75	0.09	100.87
CE0282 M	45.80	3.50	13.87	14.24	0.19	6.37	12.49	2.41	1.32	0.44	-0.64	0.11	100.10
CE0223 M	47.88	3.03	14.34	11.88	0.17	7.41	11.92	2.66	1.39	0.48	-0.60	0.08	100.64
CE0203 M	47.31	3.49	15.67	12.77	0.18	5.56	10.51	3.07	1.51	0.55	-0.76	0.06	99.92
CE0192 M	46.60	3.46	15.66	13.58	0.19	5.64	10.96	2.94	1.56	0.52	-0.78	0.05	100.38
CE0182 M	46.52	2.96	13.98	11.98	0.17	7.78	13.02	2.33	1.20	0.40	-0.39	0.09	100.04
CE0171 M	46.73	2.87	14.00	12.00	0.17	9.01	12.19	2.43	1.21	0.40	-0.40	0.07	100.68
CE0151 M	46.70	2.89	13.66	12.27	0.17	9.29	12.06	2.45	1.02	0.39	-0.37	0.09	100.62
CE0143 M	47.26	2.84	13.56	11.66	0.17	8.89	11.83	2.18	1.25	0.44	-0.12	0.13	100.09

Stratigraphic unit numbers are from J. Nougier (personal communication). AV, Albatros Valley; PF, Penguin Falls; M, Mt Marion. All samples were coarsely crushed and sieved to a 0.2–0.5 mm size fraction from which weathered and cumulative portions were removed to obtain a phenocryst-free matrix separate. These fresh rock chips were then repeatedly washed ultrasonically in ultra-purified water to remove any potential contaminants, then dried with ethanol. They were then crushed in an agate mortar and weighed. Major element chemistry was determined on ~1.2 g of powdered matrix sample by X-ray fluorescence spectroscopy using fused glass discs at the Laboratoire des Sciences de la Terre (UMR 5570), University Claude Bernard, Lyon 1. Analytical errors are less than 2% for SiO₂, Al₂O₃, Fe₂O₃, MgO, CaO, Na₂O and TiO₂, and 5–10% for MnO, K₂O and P₂O₅. The reproducibility (% RSD) for this latter technique, based on repeated analyses of four East Island samples, ranges from 0.02 to 0.33%.

CE0192 M) overlap with those obtained on the same flows by Gunn *et al.* (1970).

Evaluation of alteration

Our samples do not show any marked geochemical signs of subaerial alteration. Sodium and K are readily lost during glacial weathering of basalts, whereas Ca, Si, and P are more slowly leached (Gislason *et al.*, 1996). Aluminum, Fe, Ti, and Mn can be considered as near-immobile elements during this process (Gislason *et al.*, 1996). Overall, our samples do not display any correlations between loss on ignition (LOI) or degree of petrographic alteration and relative depletions of K₂O, Rb, Ba, Sr and Na₂O. Instead, the latter correlate with immobile elements such as Nb, Ta, and Th. Uranium, which can be mobile in some subaerial environments, generally appears to have been only little affected by secondary processes. The range of whole-rock Th/U ratios for all samples (3.9–5.3) is similar to the range (4.0–5.3) reported for the various lava series of the Crozet archipelago (Breton *et al.*, 2013) and overlaps with that of worldwide ocean island basalt (OIB) (2.8–5.3; Andersen *et al.*, 2015). Whole-rock Nd/Pb, which varies between 13.9 and 16.9, slightly extends the range of other Crozet archipelago lavas (12.9–16.1; Breton

et al., 2013) and falls in the range of modern OIB globally (9.8–21.9; Newsom *et al.* 1986), indicating that alteration-related mobility of Pb generally has been modest. The major and trace element systematics indicate that the trends observed in East Island lavas are magmatic rather than weathering-induced.

MAJOR ELEMENT CHEMISTRY

General classification of magma types

Overall, the lavas from East Island are not MgO-rich (MgO < 9 wt %, Table 2). The most magnesian rocks (MgO > 9 wt %) are phryic basalts (CE0016 PF, CE0021 PF, and CE0151 M) containing a large amount of olivine phenocrysts and a minor proportion of clinopyroxene phenocrysts, whereas the least magnesian rocks are aphyric basalts (CE0192 M and CE0203 M; see Supplementary Data Electronic Appendix 1 for petrographic and mineralogical descriptions of the East Island samples). In a total alkalis (Na₂O + K₂O) versus silica (TAS) diagram (Fig. 3), the lavas from East Island are all classified as alkali basalts and overlap with the moderately alkaline suite defined by other Crozet magmatic rocks (Chevallier *et al.*, 1983; Verwoerd *et al.*, 1990; Zhou, 1996; Breton *et al.*, 2013). Their nepheline

Table 3. Trace element data (in ppm) for lavas from East Island (Crozet Archipelago, Indian Ocean); all samples are basalts in TAS classification

	Sc	Cs	Rb	Sr	Y	Zr	Nb	Ba	Hf	Ta	Pb	Th	U	La	Ce	Pr	Nd	Sm	Eu	Gd	Tb	Dy	Ho	Er	Tm	Yb	Lu		
<i>Albatros Valley, Unit 2</i>																													
CE0106 AV	30.2	0.23	32.2	573	28	273	51.0	318	6.7	3.4	2.76	5.79	1.39	43.99	91.64	11.33	45.44	9.65	2.93	8.28	1.21	6.48	1.16	2.73	0.36	2.07	0.29		
CE0084 AV	36.3	0.46	19.1	405	23	203	37.2	253	5.2	2.5	2.19	4.01	0.97	31.32	65.60	8.25	33.95	7.37	2.31	6.57	0.96	5.22	0.95	2.26	0.30	1.68	0.24		
CE0061 AV	29.7	0.24	29.8	567	28	249	48.6	327	6.1	3.2	2.62	5.41	1.19	41.21	85.45	10.58	42.73	9.04	2.81	7.87	1.17	6.35	1.16	2.75	0.36	2.11	0.30		
CE0054 AV	28.9	0.26	26.6	549	27	242	47.1	319	6.0	3.1	2.58	5.24	1.09	40.23	83.71	10.38	41.92	8.89	2.75	7.71	1.15	6.22	1.13	2.69	0.36	2.03	0.29		
CE0041 AV	27.0	0.15	29.1	559	28	253	49.6	306	6.3	3.3	2.80	5.47	1.04	42.04	87.60	10.75	43.21	8.93	2.87	7.83	1.17	6.35	1.15	2.80	0.36	2.11	0.30		
CE0031 AV	28.5	0.27	26.5	543	27	244	47.7	298	6.0	3.2	2.74	5.20	1.12	40.89	85.42	10.55	42.18	8.78	2.78	7.66	1.14	6.20	1.11	2.72	0.36	2.03	0.30		
<i>Penguin Falls, Unit 3a</i>																													
CE0021 PF	34.5	0.42	29.2	456	24	203	38.5	277	5.1	2.6	2.24	4.19	1.05	32.50	68.50	8.54	34.96	7.55	2.43	6.73	1.00	5.41	0.97	2.30	0.30	1.70	0.25		
CE0016 PF	34.9	0.37	26.4	428	23	187	35.8	251	4.7	2.4	1.98	3.72	0.95	29.71	63.17	8.03	33.00	7.16	2.32	6.48	0.96	5.25	0.95	2.25	0.30	1.69	0.24		
<i>Mt Marion, Unit 3b</i>																													
CE0432 M	35.4	0.18	29.5	459	26	219	43.2	287	5.5	2.9	2.41	4.61	1.12	35.64	74.12	9.24	37.37	7.92	2.53	7.04	1.04	5.75	1.04	2.53	0.32	1.92	0.27		
CE0412 M	36.3	0.12	23.3	410	23	203	37.5	233	5.0	2.5	2.09	4.16	0.91	31.78	67.01	8.38	34.01	7.27	2.30	6.52	0.97	5.22	0.95	2.34	0.30	1.75	0.25		
CE0402 M	35.8	0.17	25.4	409	24	213	39.5	248	5.2	2.7	2.09	4.43	0.88	33.56	70.16	8.81	35.35	7.54	2.38	6.72	0.98	5.37	0.99	2.34	0.32	1.81	0.25		
CE0383 M	29.8	0.20	34.3	537	27	285	49.1	314	6.6	3.3	2.82	5.63	1.38	43.44	89.02	10.78	42.93	8.79	2.74	7.61	1.11	6.02	1.09	2.61	0.34	2.02	0.29		
CE0371 M	29.6	0.21	35.4	546	27	288	49.5	318	6.8	3.3	2.95	5.74	1.43	43.77	89.22	10.81	42.95	8.60	2.74	7.51	1.10	5.94	1.08	2.60	0.35	2.04	0.29		
CE0344 M	28.4	0.26	34.0	598	28	268	49.9	326	6.5	3.3	2.97	5.53	1.36	42.42	87.28	10.71	43.24	8.86	2.91	8.03	1.18	6.33	1.17	2.79	0.37	2.10	0.31		
CE032 M	31.5	0.18	25.2	542	25	233	45.2	286	5.7	2.9	2.44	4.99	1.21	38.32	78.63	9.69	38.81	8.00	2.62	7.16	1.06	5.68	1.03	2.44	0.33	1.90	0.27		
CE0303 M	32.9	0.29	31.2	508	26	246	50.9	287	6.2	3.2	2.97	5.89	1.48	38.94	80.68	9.94	39.70	8.28	2.60	7.16	1.05	5.71	1.03	2.44	0.33	1.89	0.27		
CE0293 M	32.4	0.16	28.8	499	25	221	42.5	284	5.4	2.8	2.45	4.55	1.09	35.88	74.47	9.21	37.01	7.69	2.49	6.94	1.02	5.56	1.01	2.43	0.31	1.83	0.26		
CE0282 M	31.1	0.35	31.2	539	28	244	50.9	316	6.0	3.4	2.82	5.52	1.31	41.34	85.45	10.55	42.32	8.95	2.84	7.97	1.17	6.37	1.16	2.83	0.37	2.11	0.30		
CE0223 M	33.1	0.21	34.1	576	27	266	51.7	332	6.3	3.4	2.87	5.90	1.38	44.02	89.67	10.93	43.16	8.88	2.79	7.69	1.12	6.01	1.09	2.63	0.34	1.98	0.27		
CE0203 M	25.0	0.30	34.7	614	29	287	54.6	348	6.7	3.6	2.99	6.11	1.54	46.19	97.66	11.70	46.58	9.50	2.98	8.22	1.20	6.48	1.18	2.76	0.37	2.15	0.30		
CE0192 M	24.9	0.44	38.6	628	30	293	57.7	361	6.8	3.8	3.03	6.34	1.56	46.92	98.61	11.94	47.42	9.64	3.08	8.47	1.26	6.68	1.22	2.94	0.39	2.26	0.32		
CE0182 M	41.2	0.19	25.5	486	24	207	39.9	250	5.2	2.7	2.24	4.22	0.95	32.54	69.32	8.67	35.43	7.60	2.46	6.84	1.01	5.42	0.97	2.34	0.31	1.78	0.26		
CE0171 M	34.2	0.39	29.1	528	24	218	43.6	287	5.4	2.9	2.55	4.94	1.22	36.87	76.19	9.32	37.22	7.87	2.49	6.99	1.02	5.41	0.99	2.36	0.30	1.76	0.26		
CE0151 M	31.9	0.45	23.2	520	24	218	43.2	289	5.4	2.9	2.51	5.00	1.22	36.95	76.27	9.35	37.72	7.91	2.46	6.86	1.02	5.48	0.98	2.37	0.32	1.78	0.26		
CE0143 M	31.6	0.36	31.6	529	25	244	48.1	310	5.9	3.2	2.84	5.71	1.42	41.84	85.38	10.29	40.87	8.34	2.58	7.07	1.04	5.69	1.02	2.46	0.32	1.87	0.27		

Trace element analyses were performed by inductively coupled plasma mass spectrometry (Agilent model 7700X) on ~1 g of powdered matrix sample following the routine procedure used at the Geoanalytical Laboratory at Washington State University. Long-term precision (% RSD) for the method is typically better than 10% for trace elements and 5% for the lanthanide REE. The reproducibility, as judged by replicate dissolution ($n = 54$) of the BCR geostandard over a 3 year period, is 0.9–2.1% for lanthanide REE and 0.8–9.5% for trace elements (Ba, Th, Nb, Y, Hf, Ta, U, Pb, Rb and Cs). (See Table 2 for abbreviations.)

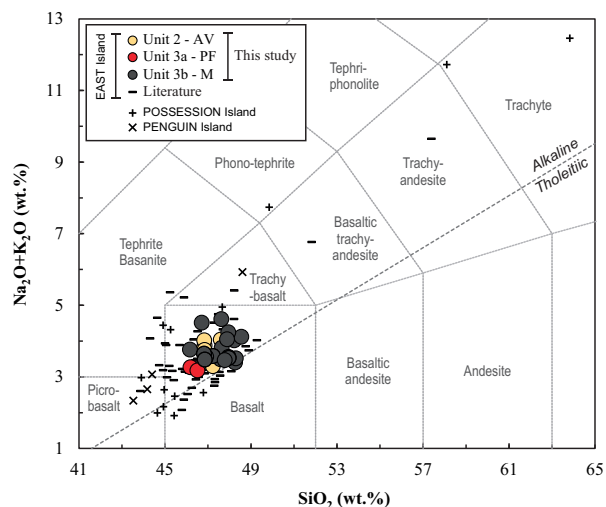


Fig. 3. Total alkalis vs SiO_2 (wt %) classification (TAS; Le Bas *et al.*, 1986) for samples from East Island and other islands of the Crozet archipelago. The alkaline–tholeiitic discrimination boundary of Macdonald (1968) is indicated. Literature data for East Island (short line symbols) are from Gunn *et al.* (1970), Chevallier *et al.* (1983) and Zhou (1996). Data for Possession Island are from Chevallier *et al.* (1983), Verwoerd *et al.* (1990) and Breton *et al.* (2013). Data for the western group of islands are from Bellair (1963) for Pig Island and from Breton *et al.* (2013) for Penguin Island. AV, Albatros Valley; PF, Penguin Falls; M, Mt Marion.

normative contents (calculated volatile free after normalization to 100% and assuming $\text{Fe}_2\text{O}_3/\text{FeO} = 0.11$, after Cottrell & Kelley, 2011), varying from 0.3 to 4.4 for most of the samples, further confirm their alkalic nature. Only one sample (CE0032 M) is slightly hypersthene normative.

Major element variations as a function of MgO

When major element chemistry is considered as a function of MgO (Fig. 4), our results generally overlap with previously published whole-rock data for the Crozet archipelago (Bellair, 1963; Gunn *et al.*, 1970; Chevallier *et al.*, 1983; Zhou, 1996; Breton *et al.*, 2013); however, at a given MgO content, the variation of major element concentrations within our dataset is generally small compared with that of previous studies. Decreasing MgO content is associated with an increase in Al_2O_3 , TiO_2 , Na_2O , K_2O , and P_2O_5 (Fig. 4). In contrast, SiO_2 , FeO , and CaO show little, if any, systematic variation as a function of MgO (Fig. 4). We note that these variations are qualitatively consistent with the trends expected for liquid lines of descent resulting from crystallization of olivine + clinopyroxene (Fig. 4). At the scale of the archipelago, for a given MgO content, there are some systematic compositional variations between the eastern and western groups of islands. Lavas from the western group are on average richer in FeO and TiO_2 , but poorer in SiO_2 and CaO relative to those from the eastern group. At a given MgO content, the compositions of lavas from Possession Island differ from those of East Island in having lower Na_2O and SiO_2 , and slightly higher Al_2O_3 .

TRACE ELEMENT CHEMISTRY

Primitive mantle normalized trace element abundances

The abundances of trace elements in the studied East Island lavas are presented in Table 3. Relative to an estimated primitive mantle composition, the trace element abundance patterns of East Island lavas are typical of within-plate volcanic rocks, showing enrichments in Nb and Ta (Fig. 5a; Willbold & Stracke, 2006). One distinctive feature of these patterns is their negative K anomaly with respect to Ta and La (Fig. 5a). Other large ion lithophile elements (LILE), such as Ba and Rb, are also depleted relative to Th in East Island samples, whereas Sr does not display a negative anomaly relative to Nd and Zr (Fig. 5a).

When incompatible element abundances for all units of East Island are normalized to an estimated primordial mantle composition, some basalts potentially belonging to Unit 1 (Zhou, 1996) display slightly higher abundances of highly incompatible elements and lower abundances of moderately incompatible elements relative to those of Units 2 and 3 (Fig. 5b). Lavas from Possession Island show slightly stronger fractionation of highly incompatible relative to moderately incompatible elements, and have lower overall abundances of moderately incompatible elements (Fig. 5b and c). We note that the trace element abundances of Possession Island lavas have a smaller range of variation than those of East Island (Fig. 5b). In contrast, lavas from Penguin Island show geochemical differences relative to those of the oldest islands, which are illustrated by the presence of a larger positive Nb–Ta anomaly, with the concurrent development of large positive Ba and Sr anomalies relative to Rb–Th and Nd–Zr (Fig. 5b and c; Breton *et al.*, 2013). Another distinctive feature of these lavas is their overall lower abundances of trace elements compared with the older group, with the most highly incompatible elements from Rb to U being the lowest.

Rare earth elements

Chondrite-normalized rare earth element (REE) patterns for the studied lavas are broadly subparallel and show a steady decrease from La to Lu with no discernible negative Eu or Ce anomalies (Fig. 6a). The near-absence of Eu anomalies is consistent with the small amount of plagioclase phenocryst crystallization observed in East Island rocks. The light REE (LREE) exhibit slightly greater variations than the heavy REE (HREE) (Fig. 6a). Our REE element data overlap with data obtained for other alkali lavas of East Island (Zhou, 1996; Breton *et al.*, 2013). With the exception of two samples potentially belonging to Unit 1 of East Island (Zhou, 1996), all lavas from the Crozet archipelago broadly exhibit subparallel REE patterns, with most of those from Possession and Penguin Islands having lower abundances of REE than East Island lavas (Fig. 6b and c; Breton *et al.*, 2013).

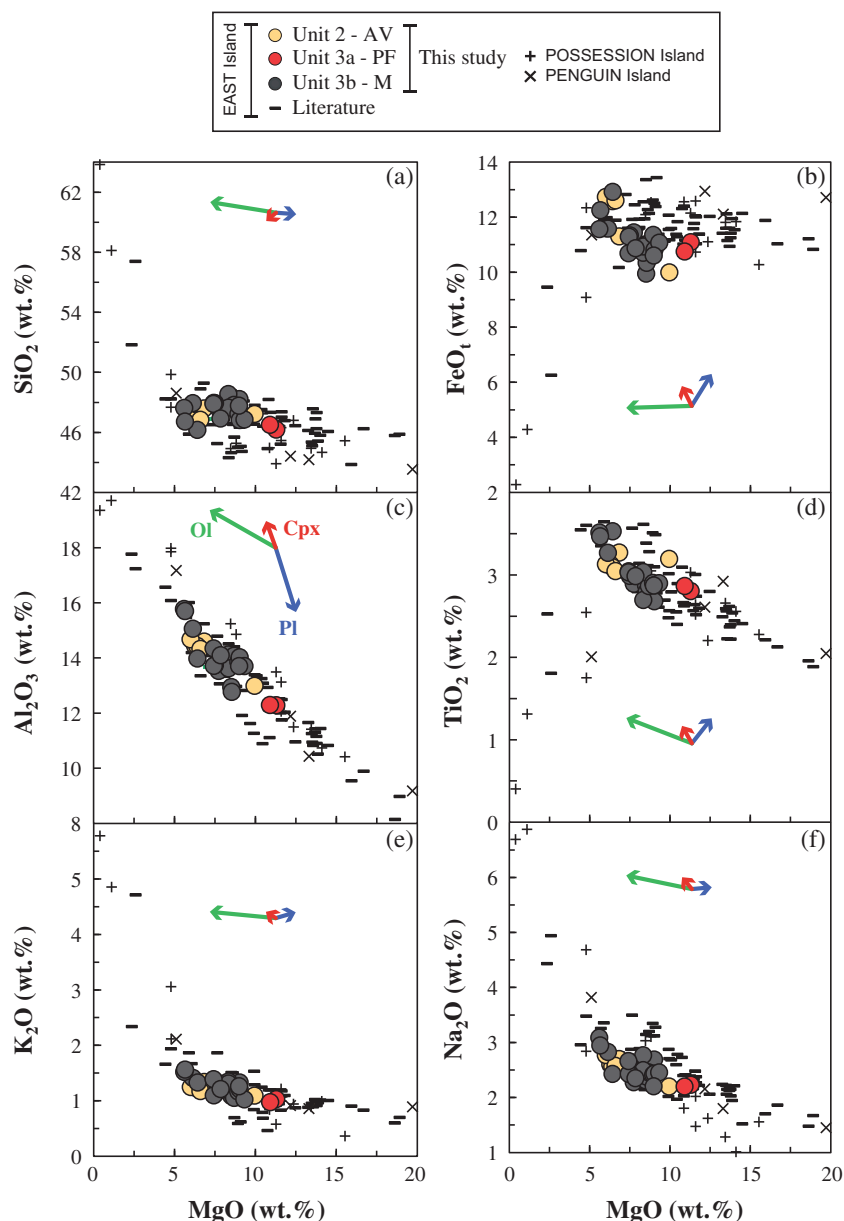


Fig. 4. Major element variation (wt %) vs MgO (wt %) for lavas from East Island and other islands of the Crozet archipelago. Major element data have been recalculated to 100 wt % volatile-free. Data sources as in Fig. 3. Colored vectors indicate the effect of 10% crystallization of olivine (Ol), plagioclase (Pl) and clinopyroxene (Cpx) on a melt with about 11 wt % MgO. (a) SiO₂ vs MgO; (b) FeO_t vs MgO; (c) Al₂O₃ vs MgO; (d) TiO₂ vs MgO; (e) K₂O vs MgO; (f) Na₂O vs MgO.

DISCUSSION

Evaluating the effect of differentiation processes

All East Island lavas analyzed in this study are interpreted to have experienced variable degrees of crystal fractionation or accumulation since segregation from their mantle source regions. The abundance of phenocrysts in East Island lavas indicates that their magmas erupted as crystal–liquid mixtures, with the exception of rare aphyric samples. The average bulk composition of magma batches primarily reflects crystal–liquid dynamics in the magma reservoir system. The abundance, size, and shapes of the phenocrysts require that olivine and clinopyroxene were well-established liquidus phases in the magmas prior to eruption. The occurrence of isolated

plagioclase microphenocrysts, phenocrysts (CE0293 M), or glomeroporphyritic clots in some lavas indicates that plagioclase was also, occasionally, a liquidus phase. The observed major element variations in the residual liquids are qualitatively consistent with the dominant control of olivine and clinopyroxene on the liquid lines of descent as shown by the mineral vectors in Fig. 4. As observed in many basaltic suites, olivine control is predominant during the early stage as defined here by a group of samples (CE0084 AV, CE0016 PF, CE0021 PF, CE0412 M and CE0402 M). Variations in CaO, SiO₂, and FeO between 9 and 5 wt % MgO clearly indicate that olivine is not fractionating alone (Fig. 4). The marked negative correlation observed in CaO/Al₂O₃ as a function of FeO/MgO (Fig. 7a)

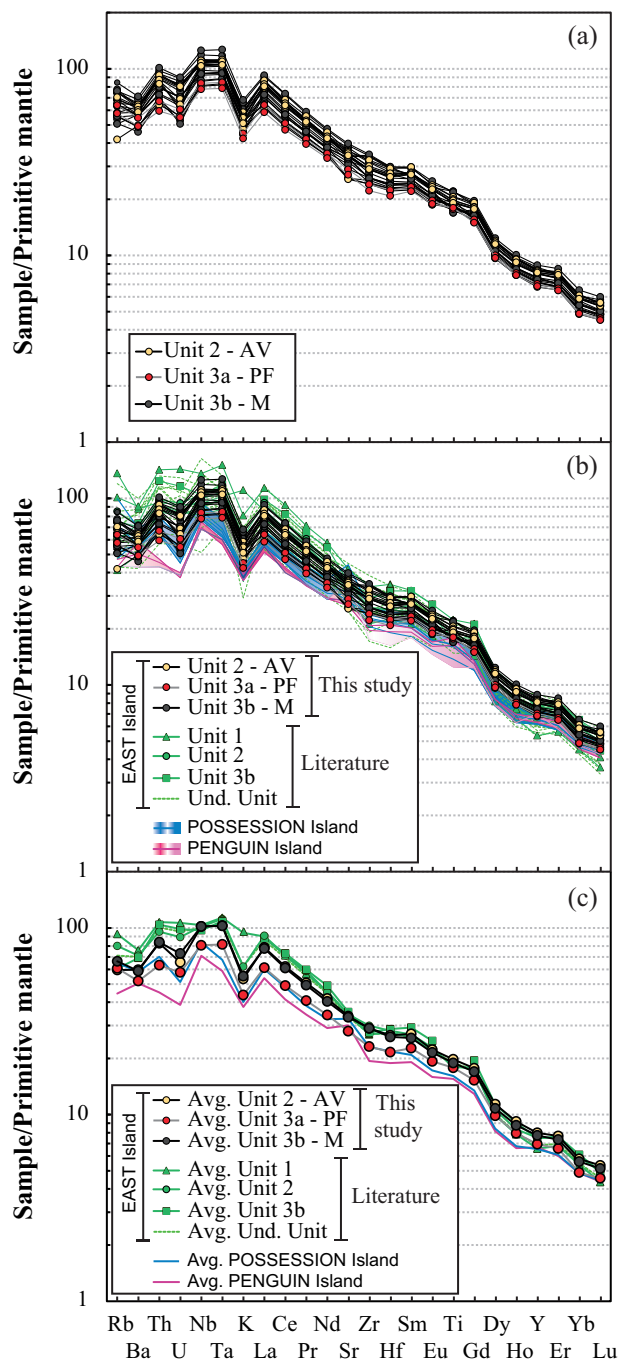


Fig. 5. Trace element concentrations in lavas from East Island, and other islands of the Crozet archipelago normalized to the primitive-mantle values of Lyubetskaya & Korenaga (2007). (a) Units 2, 3a and 3b of East Island (this study); (b) shown for comparison are samples from East Island (literature), Possession and Penguin Islands; (c) average (Avg) compositions for lavas shown in (a) and (b). Data sources as in Fig. 3. AV, Albatros Valley; PF, Penguin Falls; M, Mt Marion.

indicates that clinopyroxene exerts a dominant control on the liquid evolution. Additional evidence for its dominant fractionation is provided by a plot of Sc versus $\text{CaO}/\text{Al}_2\text{O}_3$ (Fig. 7b), which shows a pronounced kink at $\text{CaO}/\text{Al}_2\text{O}_3$ of 0.9. Scandium is a trace element compatible in clinopyroxene but not in olivine. We note that the data do not define

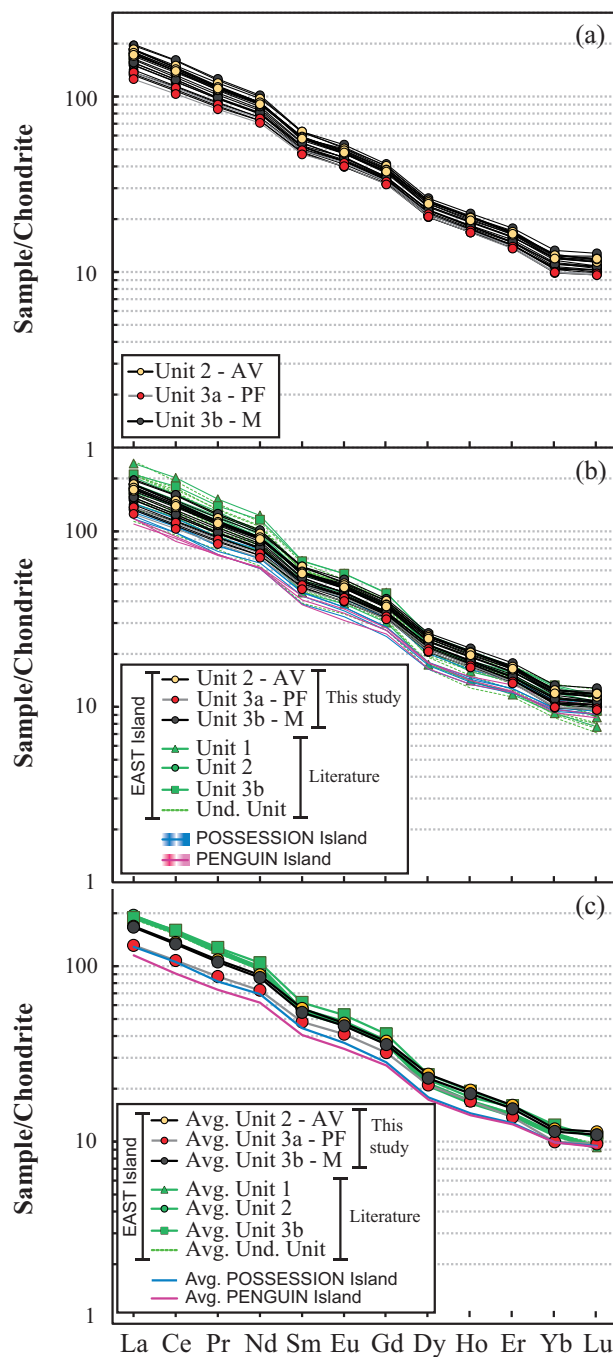


Fig. 6. REE data for East Island lavas and other islands of the Crozet archipelago normalized to the chondritic values of Sun & McDonough (1989). (a) Units 2, 3a and 3b of East Island (this study); (b) shown for comparison are samples from East Island (literature), Possession and Penguin Islands; (c) average (Avg) compositions for lavas shown in (a) and (b). Data sources as in Fig. 3. AV, Albatros Valley; PF, Penguin Falls; M, Mt Marion.

any linear array between two end-members that could be interpreted as the result of mixing between two compositionally distinct magmas.

Pressure of crystallization

We determined the diopside–melt equilibration P – T for three samples (CE0031 AV, CE0344 M, and CE0203 M)

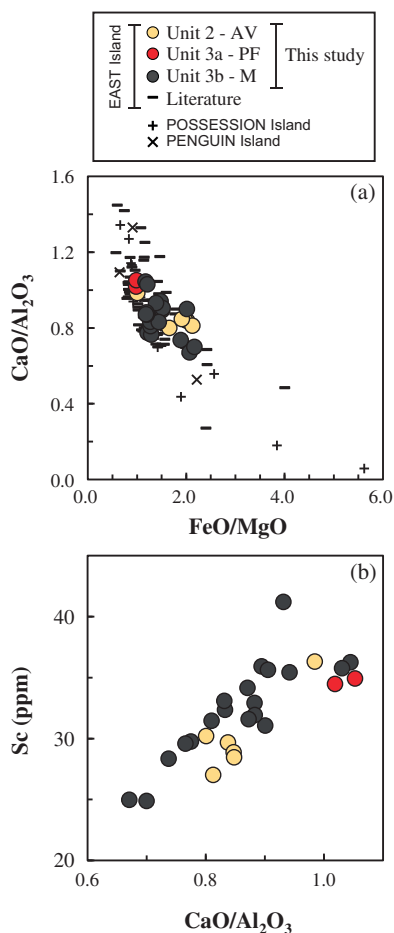


Fig. 7. Variations in $\text{CaO}/\text{Al}_2\text{O}_3$ vs FeO/MgO (a) and Sc (b) for lavas from East, Possession and Penguin Islands (Crozet archipelago). Data sources as in Fig. 3.

using the clinopyroxene–melt equilibrium thermobarometer of Putirka *et al.* (1996), which was calibrated using experimentally produced melt compositions and the proportion of the jadeite component in the coexisting clinopyroxene. For each sample, only a single pressure estimate is provided for what is probably a polybaric crystallization path. Using the preferred equations of Putirka *et al.* (P1 and T2), under anhydrous conditions, we find that the compositions of clinopyroxene phenocryst rims or microphenocrysts in equilibrium with residual melt were last equilibrated at 6.1 ± 0.5 kbar (21.4 ± 1.8 km) and $1179 \pm 6^\circ\text{C}$, providing evidence for some extent of crystallization at high pressures within the uppermost mantle as the Moho depth has been estimated at about 10–12 km below the eastern Crozet Bank (Recq *et al.*, 1998). A similar magma plumbing system, with major fractionation of magmas occurring within the uppermost mantle, has been reported beneath the Cape Verde, Kerguelen, Madeira and Canary islands (e.g. Amelung & Day, 2002; Damasceno *et al.*, 2002; Schwarz *et al.*, 2004; Longpré *et al.*, 2008). If hydrous conditions are considered, the equilibration pressures and temperatures (e.g. Putirka, 2008) are within error of those obtained in anhydrous

environments. Although not shown, calculations of the liquid lines of descent performed using the PETROLOG program of Danyushevsky & Plechov (2011) and the partition coefficients for phase equilibria of Ariskin *et al.* (1993) confirm the crystallization of olivine and clinopyroxene between 4 and 6 kbar and reproduce the natural basaltic trends. Such high-pressure liquid lines of descent lead to significant increases in Al_2O_3 with decreasing MgO, as observed in Fig. 4. However, the studied samples have undergone a very small amount of low-pressure crystallization, in addition to some crystal accumulation, which could account for the dispersion generally observed between the major chemical differentiation indices, as demonstrated by the presence of plagioclase phenocrysts in some samples (e.g. CE0203 M).

Fractionation of amphibole and phlogopite

In Fig. 8, the samples from East Island form a scattered group in K_2O – SiO_2 space, suggesting buffering of K_2O by a K-bearing phase such as amphibole or phlogopite during magmatic differentiation. However, owing to the low $P_{\text{H}_2\text{O}}$ of alkaline magmas, early crystallization of amphibole and phlogopite is rather unlikely. None of these minerals have been identified in East Island lavas, but most plutonic rocks from the basement unit (ultramafic cumulates to syenitic rocks; Zhou, 1996) have phlogopite- and/or amphibole-bearing parageneses. In addition, some investigators have recently recognized the presence of kaersutite in differentiated samples from Possession Island (trachybasalt, trachyandesite, trachyte and tephri-phonolite; Segard *et al.*, 2011). Both phlogopite and kaersutite will preferentially incorporate Al_2O_3 , K_2O and TiO_2 relative to olivine and clinopyroxene. Kaersutite will also favor the incorporation of middle REE (MREE) (Gd to Ho) over HREE (Er to Lu; Tiepolo *et al.*, 2007). Its fractionation tends to produce MREE–HREE patterns that are concave upward ('spoon'-shaped). This shape is not observed in the REE patterns of our samples (Fig. 6). The crystallization of phlogopite should produce a decrease in K_2O with increasing SiO_2 in the residual liquid, in contrast to the near-constant K_2O with increasing SiO_2 observed in our data (Fig. 8).

Are there any primary magma compositions in East Island that can be used to evaluate mantle potential temperature?

First, we have to evaluate whether any of the samples with MgO exceeding 10 wt % can be regarded as the primary products of mantle melting. Because liquid lines of descent are poorly defined in East Island samples, fitting least-squares regression lines to element concentrations to subtract the effect of fractional crystallization (e.g. Klein & Langmuir, 1987) on primitive liquid compositions does not constitute a rigorous approach. Most other methods used to estimate the composition of a primary magma are subject to strict limitations. Their validity holds only if applied to lavas from which solely

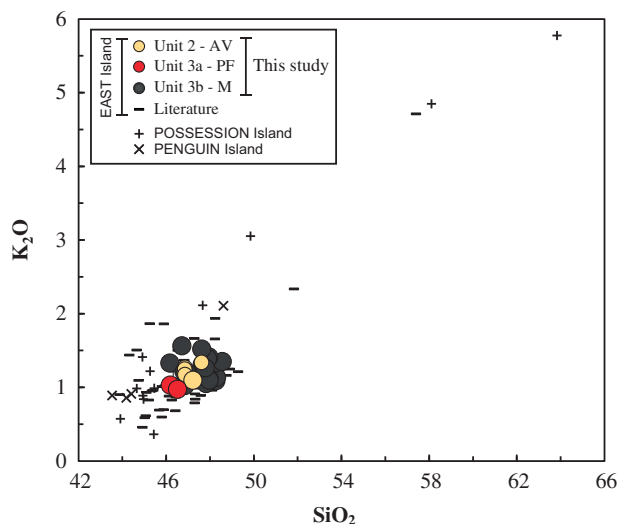


Fig. 8. K_2O vs SiO_2 (wt %) for lavas from East, Possession and Penguin Islands (Crozet archipelago). Data sources as in Fig. 3.

olivine has crystallized, as they require incremental addition or subtraction of olivine to obtain the primitive magma composition (Putirka, 2005; Herzberg *et al.*, 2007; Humphreys & Niu, 2009; Dasgupta *et al.*, 2010). None of our samples meet this criterion. The only sample with MgO content exceeding 10 wt % and with less than 10% crystals, CE0021 PF, contains some clinopyroxene and olivine phenocrysts.

Estimating mantle potential temperature from reconstructed primary magma compositions for East Island samples using olivine–liquid equilibrium thus appears to be a rather imprecise exercise. Regardless, olivine–liquid equilibrium has been used by Putirka (2008) to reconstruct the average primary magma composition of East Island lavas from the highly phyrlic suite (e.g. ankaramites and oceanites) collected by Gunn *et al.* (1970). As these contain a large amount of clinopyroxene and olivine crystals, they cannot be considered as parental liquids. We nevertheless use their average composition to quantify and place some limits with PRIMELT2 (Herzberg & Asimow, 2008) on the range of potential temperatures associated with their genesis and compare these results with those obtained by Putirka (2008).

Using the average of Gunn's samples with 10–15 wt % MgO, Putirka (2008) inferred an average mantle potential temperature of 1542°C, whereas the PRIMELT2 model estimates a lower temperature of 1466°C (reflecting ~5% accumulated melting of a garnet-bearing lherzolite) for the same composition (with Fe_2O_3/TiO_2 ratio of unity). In addition to being phyrlic, some samples (CE0016 PF and CE0021 PF) could be CO_2 -bearing primary melts, as defined by the empirical filter of Herzberg & Asimow (2008). PRIMELT2 also allows filtering out the chemical fingerprint of clinopyroxene accumulation. After having filtered out these samples for these two effects, the PRIMELT2 program estimates almost the same potential temperature of ~1465°C, but a

slightly higher accumulated fractional melting extent of ~7.5%.

Using PRIMELT2, estimations of average mantle potential temperatures for the lava suite of Gunn *et al.* (1970) of 1465–1466°C place the Crozet 'hotspot' among those having the lowest mantle potential temperature (e.g. Azores, Canary Islands), although still higher than the nominal values of the average ambient mantle. We note that thermally weak hotspots (Azores, Canary; Herzberg & Gazel, 2009) are often located in motionless plate environments. However, such mantle potential temperatures should be considered with great caution. First, we cannot convincingly demonstrate that any of the MgO-rich samples from Gunn *et al.* (1970) are representative of high-MgO and hence primary melts. Second, although error propagation to account for the accumulation of clinopyroxene does not appear to strongly bias the estimation of the parental magma composition, and hence that of the mantle potential temperature, the same is not true for the effects of volatiles (H_2O and CO_2 , Sisson *et al.*, 2009), alkaline elements (Hirschmann, 2000; Brey *et al.*, 2011), oxides and residual garnet.

What role do assimilation processes play in the genesis of East Island lava compositions?

The assimilation of small crustal fragments results in the addition or dissolution of xenoliths or xenocrysts from magmatic or hydrothermal units into the magma and possibly in the formation of peritectic crystals (Erdmann *et al.*, 2010). Dissolution of common ultramafic xenocrystic minerals (olivine, clinopyroxene, and orthopyroxene) in basaltic magmas is usually minimal and likely to be significant only if the xenolith is small, and the magma is superheated by more than 50°C (Brearley & Scarfe, 1986). Regardless, we evaluate the chemical contribution of assimilation of crustal fragments to the chemistry of the East Island lavas, especially as some samples recently collected on Possession Island contain xenolithic inclusions (Segard *et al.*, 2011).

Potential evidence for assimilation is provided by the occurrence of olivine phenocrysts in Crozet lavas that are out of equilibrium with the groundmass [$K_d(Fe-Mg)_{Ol-liquid} \neq 0.3 \pm 0.03$] and exhibit deformation banding (see Supplementary Data Electronic Appendix 1 for a full mineralogical description). However, their chemistry does not differ from that of undeformed phenocrysts (see Supplementary Data Electronic Appendices 1 and 2). Dislocation-bearing olivine crystals, containing inclusions of magmatic spinel or chromite, have also been found in dunite xenoliths at East Island (Zhou, 1996). As observed at Hawaii and Reunion islands (Garcia, 1996; Albarède *et al.*, 1997), these olivines may either be derived from mechanical disaggregation of earlier cumulates crystallizing at the base of a magma chamber or have been deformed as the magma flowed through narrow conduits at elevated pressure. The observation

of clinopyroxene phenocrysts in high-MgO lavas (>10 wt %), which at low pressure are saturated with only olivine and minor chromian spinel, further suggests either mixing with or assimilation of more evolved liquids produced at moderate pressure or with cumulates produced at high pressure.

Because of their low melting temperatures (e.g. Mengel & Green, 1989; Foley *et al.*, 1999), volatile-bearing minerals (amphibole, phlogopite, and apatite), as well as ilmenite, will be the earliest minerals to be consumed during melt–rock interaction. Their trace element budget may therefore be transferred to the host primary magmas. Most rocks from the plutonic basal unit (e.g. wehrlite, gabbro, monzogabbro, monzodiorite, monzonite and syenite; Zhou, 1996) of East Island contain as accessory phases: mica (phlogopite/biotite) and/or minor calcic amphibole (kaersutite, hastingsite, ferropargasite, pargasite and magnesiohornblende), Fe–Ti oxides (ilmenite) and apatite. The paragenesis of differentiated rocks (trachybasalt, trachyandesite, tephriphonolite, trachyte and phonolite) recently described at Possession Island also includes some kaersutite (Segard *et al.*, 2011).

Apatite addition or dissolution should lead to marked enrichments in P₂O₅, Th, U, Sr and REE relative to high field strength elements (HFSE; Nb, Ta, Zr, and Hf) (Prowatke & Klemme, 2006). None of these trace element fingerprints are observed in our samples (Fig. 5). Ilmenite dissolution should impose some overprints on host liquids for TiO₂, Pb, Nb, Ta, Zr, and Hf relative to REE (Klemme *et al.*, 2006). High levels of TiO₂, Nb, and Ta (Fig. 5) are not found in our samples. Above all, addition of ilmenite will induce a positive correlation between TiO₂ and MgO contents, which is not observed (Fig. 4). Assimilation of phlogopite or amphibole crystals (up to 10%) will have a small effect on major element systematics. The dissolution of phlogopite will both decrease CaO and increase Al₂O₃ and K₂O abundances with increasing MgO in the host liquid. The opposite systematics observed in the East Island lavas rule out such a process (Fig. 4). Significant amounts of Rb and Ba should be transferred to the melt, but no positive anomalies are observed in the normalized trace element patterns of our samples (Fig. 5). The dissolution of amphibole xenocrysts will increase Na₂O, TiO₂, Nb, and Ta contents with increasing MgO in the host liquid. None of these chemical characteristics are present in our dataset.

Fluids released by the breakdown of the volatile-bearing minerals included in the plutonic rocks of East Island may also have the effect of lowering their solidus temperature. Mixing in minor proportions of a plagiogranite melt derived from hydrous partial melting of wall-rock gabbro (Koepke *et al.*, 2004; France *et al.*, 2010; Wolff *et al.*, 2013) with the host magma will not alter its bulk trace element composition because of the low trace element contents (Gerlach *et al.*, 1981; Pedersen & Malpas, 1984). However, such a mixing process should lead to decreasing TiO₂ and increasing

SiO₂ abundances with decreasing MgO. Such trends are not defined by our data (Fig. 4). Wehrlite assimilation seems an unlikely process as it gives rise to ultracalcic melts (e.g. Kamenetsky *et al.*, 1998). Melting of dioritic sources will produce granodioritic to tonalitic melts with high CaO, TiO₂, Fe, Na/K, and Ca/K, and low K (Beard *et al.*, 1994). Such elemental systematics are not observed in our samples. Although no experimental data are available for syenite melting, such a process should give rise to silicic melts significantly enriched in SiO₂, K₂O and Na₂O and strongly depleted in CaO, TiO₂ and FeO (Harris & Bell, 1982). No depletion in Fe or Ti is observed in our lavas.

Garnet fingerprint: pyroxenite or garnet lherzolite?

Below the Crozet archipelago, the lithosphere might be thicker than predicted (>86 km; see Supplementary Data Electronic Appendix 1) by thermal cooling plate models, because of heat loss owing to a weakly buoyant mantle upwelling and stagnant accumulation of residual mantle material. The termination of melting at greater depth, in decreasing the melting extent, might favor a larger sampling of fertile mantle lithologies such as eclogite or garnet bearing-pyroxenite, owing to their lower solidus temperatures and higher melt productivities relative to peridotites (e.g. Hirschmann & Stolper, 1996; Ito & Mahoney, 2005a, 2005b; Sobolev *et al.*, 2005; Grove *et al.*, 2013; Shorttle *et al.*, 2014).

The attractiveness of pyroxenite or eclogite as one of the main source components for OIB resides in their potential to act as ancient and heterogeneous geochemical reservoirs (e.g. Hirschmann & Stolper, 1996; Jacob *et al.*, 2005). However, eclogite xenoliths are distinct from their pyroxenite counterparts because of their potentially protracted and complex thermo-tectonic evolution, primary occurrence in cratonic settings, bimodal mineralogy (omphacite–diopside and pyrope), trace element compositions (e.g. depletion of LREE relative to HREE, Eu and Sr anomalies and Zr depletion relative to Sm) and highly heterogeneous present-day Sr–Nd–Hf isotope signatures beyond the range of modern-day convecting mantle-derived melts (Jacob *et al.*, 2005; Gonzaga *et al.*, 2010). At least 50% of worldwide eclogite xenoliths analyzed to date display Sr and Eu anomalies (e.g. Jacob, 2004). Eclogite-derived melts are thus expected to have high values of (La/Yb)_n (because of the presence of residual garnet), to show a depletion in Zr relative to Sm, and positive Sr and Eu anomalies (Jacob, 2004; Gonzaga *et al.*, 2010). These latter anomalies are not observed in East Island lavas (Fig. 5), making it unlikely that these lithologies could significantly contribute to their mantle source.

Pyroxenites could act as another component of the East Island mantle source because of their younger age, greater heterogeneity in terms of trace and major element compositions and relatively more homogeneous present-day Sr–Nd–Hf isotope signatures,

encompassing those observed for OIB (Bizimis *et al.*, 2005, 2013; Gonzaga *et al.*, 2010). Pyroxenite xenoliths are commonly interpreted as being either the products of high-pressure segregation of mantle melts or remnants of recycled oceanic crust (Allègre & Turcotte, 1986; Kornprobst *et al.*, 1990; Gonzaga *et al.*, 2010). Here, we focus on pyroxenite samples equilibrated at high pressures from the orogenic massifs of Beni Bousera and Ronda that have been interpreted as high-pressure melts derived from precursor recycled oceanic crust (Pearson *et al.*, 1993). Many of these samples show both positive Eu and Sr anomalies (Pearson *et al.*, 1993; Garrido & Bodinier, 1999; Gysi *et al.*, 2011) and have lower contents of highly immobile incompatible elements (e.g. Th, Nb, Ta and La) relative to those of primitive mantle (Garrido & Bodinier, 1999; Gysi *et al.*, 2011). When considering as a source the pyroxenite B44 (modal proportion: 0.2 clinopyroxene and 0.8 garnet; Gysi *et al.*, 2011), the most enriched in highly incompatible elements of these suites, the liquids produced by batch melting never achieve the enrichment level in highly incompatible elements (e.g. Th, Nb, Ta and La) observed in East Island lavas whatever the melting degree and whatever the set of partition coefficients used for clinopyroxene and garnet (Salters & Longhi, 1999; Van Westrenen *et al.* 1999; Salters *et al.*, 2002; Tuff & Gibson, 2007). Further evidence against a pyroxenite component in the source of East Island lavas is provided by the CaO–MgO peridotite–pyroxenite discrimination diagram of Herzberg & Asimow (2008). Although not shown, our most primitive lavas (CE0021 PF and CE0016 PF), either corrected or uncorrected for olivine fractionation, systematically plot within the field defined by peridotite melts. All this evidence negates pyroxenite as a major component of the East Island mantle source.

As mentioned above, as the lithospheric lid might be thicker than 86 km, this limits the level to which the plume may ascend and so restricts magma generation to melting depths at which garnet is stable. Hence, although none of our lavas can be considered as primary, we compare the geochemical composition of the most magnesian lava CE0021 PF of our suite, with a crystal content of less than 10%, with the compositions of experimental liquids produced by melting of KR4003 garnet-peridotite (Walter, 1998). To allow a direct comparison, the composition of this sample has been normalized by incrementally adding olivine in equilibrium with its bulk composition, until the latter coexists with an olivine of composition Fo₉₂. This value corresponds to the mid-range of the residual olivine compositions in the set of melting experiments on KR4003 (Walter, 1998). When the variations of two melting regime barometers such as FeO and Al₂O₃ are examined its composition overlaps with those of 4.0 GPa experimental liquids from KR4003 to the right of the clinopyroxene-out line (Fig. 9), suggesting that this sample last equilibrated with a residual garnet lherzolite. This is consistent with an initiation of melting at a depth greater than

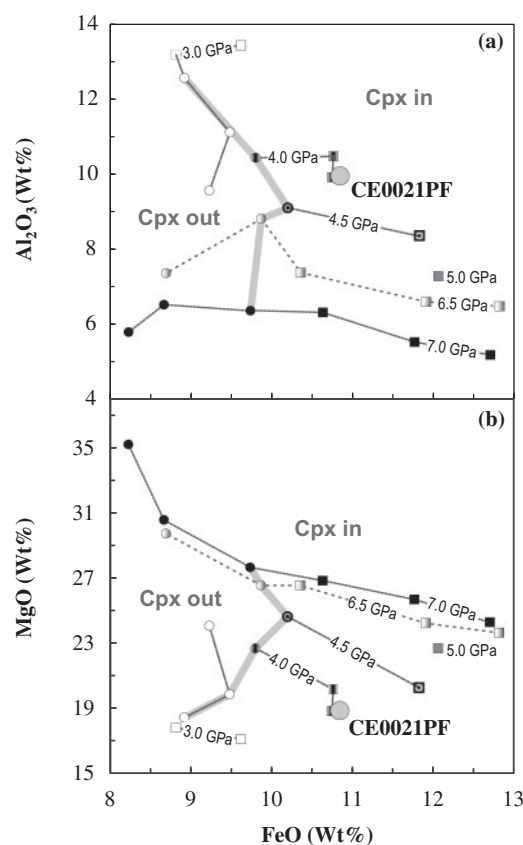


Fig. 9. Compositions of sample CE0021PF in plots of Al₂O₃ and MgO vs FeO (wt %) compared with those of liquids produced in melting experiments on KR4003 garnet-peridotite at 3.0, 4.0, 4.5, 5.0, 6.5 and 7.0 GPa (Walter, 1998). KR4003 is close in composition to the peridotites from Kilbourne Hole (KLB1) and Zabargad, the latter representing fertile oceanic upper mantle (Walter, 1998). The lava composition was modified by addition of olivine in equilibrium with the bulk magma composition until it reached a composition in equilibrium with olivine of composition Fo₉₂. This value corresponds to the mid-range of residual olivines in the set of melting experiments on KR4003. The squares denote experiments for which clinopyroxene (Cpx) is residual, whereas the circles indicate experiments in which it has been exhausted. The thick gray line separates these two fields ('Cpx in' to the right, 'Cpx out' to the left). (a) Al₂O₃ vs FeO; (b) FeO vs MgO.

that estimated for the base of the lithosphere below Crozet. It confirms that melting proceeds to small degrees within the garnet stability field, as observed for most OIB (e.g. Willbold & Stracke, 2006; Niu *et al.*, 2011). The presence of residual garnet during melting is further demonstrated by the high values of the average (Sm/Yb)_n ratio (where the subscript n indicates chondrite-normalized values) (~4.48) of East Island lavas, as well as those of the western group of islands, which exceeds unity more than fourfold and lies at the high end of the (Sm/Yb)_n–lithosphere age global positive correlation defined by OIB (Fig. 10; Humphreys & Niu, 2009; Niu *et al.*, 2011). The (Sm/Yb)_n ratio is considered as a proxy of the garnet signature in OIB melts (Hirschmann & Stolper, 1996; Putirka, 1999; Niu *et al.*, 2011).

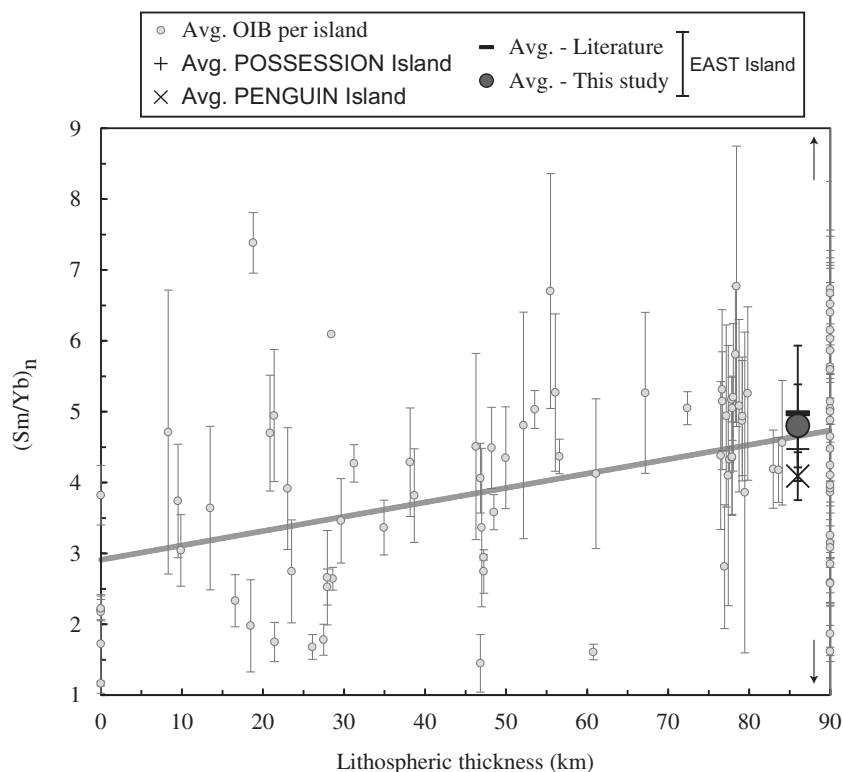


Fig. 10. Island-averaged $(\text{Sm}/\text{Yb})_n$ ratios normalized (n) to C1 chondritic values (Sun & McDonough, 1989) vs oceanic lithosphere thickness (km). Averages (Avg.) for East, Possession and Penguin Islands are from the data of Breton *et al.* (2013) and Zhou (1996). Averaged values of $(\text{Sm}/\text{Yb})_n$ and lithosphere thicknesses for other islands are from Humphreys & Niu (2009).

To summarize, at this stage of the reasoning, the trace and major element data seem to indicate that East Island lavas were derived by partial melting of a garnet-bearing lherzolite. Comparison of the trace element systematics of East Island lavas with those of liquids derived by partial melting of pyroxenite and eclogite starting materials reveals that they are not viable source lithologies for East Island lavas.

LILE depletion at East Island: a local geochemical feature?

Although none of our lavas can be considered as primary magmas, we have normalized the average composition of East Island lavas by the stepwise (~ 0.1 wt %) addition of olivine, in equilibrium with their bulk compositions, until the bulk compositions reach a Mg# in equilibrium with Fo_{88} , which corresponds to the maximum olivine forsterite content observed in our samples (see Supplementary Data Electronic Appendix 2). The normalization procedure used is that described by Herzberg & Asimow (2008). The amount of olivine crystallization derived from the calculation is used to correct the contents of the trace elements that are assumed to be perfectly incompatible in olivine. This normalization aims to provide a common point for comparing the mean composition of our alkali basalts with those of St Helena (HIMU), Tristan and Gough (EMI), Samoa and Society (EMII) and other Indian Ocean island lavas on a mantle-normalized trace element diagram (Fig. 11).

The average trace element abundance pattern of our East Island sample suite shows overall lower levels in LILE (Rb, K, Ba and Pb) in comparison with other enriched mantle (EM) OIB locations (Tristan, Gough and Society), with the exception of Samoa (Fig. 11a). The same is true for Possession Island alkali basalts (Fig. 11), which are similar to the East Island basalts (Fig. 11b). This is consistent with the earlier conclusions of Chevallier *et al.* (1983), who stated that both Possession and East Island lavas might represent the products of activity of the same volcano for more than ~ 8 Myr. As the K anomaly is seen in all East Island samples (Fig. 5a), irrespective of their silica content (e.g. Fig. 8), this implies that this anomaly is neither an artefact of the plotting procedure (e.g. Woodhead, 1996) nor a feature of low-pressure crystal fractionation in the crust. The same holds for other LILE depletions, which define flat arrays as a function of SiO_2 . In contrast, the average trace element abundance pattern for Penguin Island in the western group is enriched in Ba relative to Rb and Th and in Sr relative to Zr compared with those of the eastern group of islands (Fig. 11b). It also exhibits a larger positive Nb–Ta anomaly and overall lower abundances of trace elements compared with the older group (Fig. 11b). The age of the sampled unit from Penguin Island is ~ 1.06 Ma (Giret *et al.*, 2002; Breton *et al.*, 2013), which falls in the age interval (0.9–1.6 Ma; Verwoerd *et al.*, 1990) spanned by Unit 2 of East Island. This nearly synchronous occurrence of distinctive trace

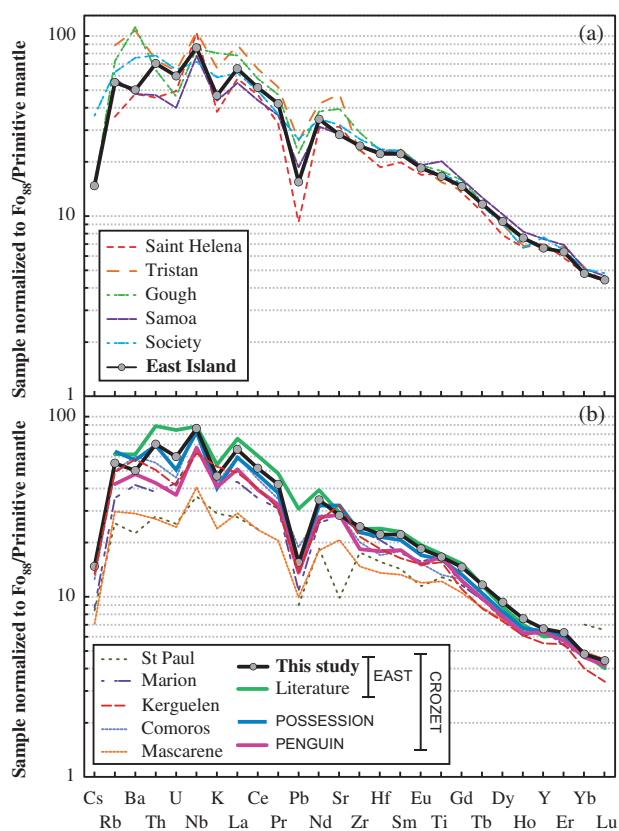


Fig. 11. Average primitive mantle normalized trace element spectrum of samples from East Island (a) compared with those of typical HIMU (St Helena), EM1 (Tristan and Gough) and EM2 (Samoa and Society) OIB; (b) compared with those of other Indian Ocean island basalts (St Paul, Marion–Prince Edward, Kerguelen, Comoros and Mascarene). The dataset used for alkali oceanic island basalts was filtered for loss on ignition (LOI) of less than 1.2 wt % to ensure that LILE variations are of primary magmatic origin. The database is composed of 186 analyses of alkali basalts *sensu stricto* [as defined by the TAS diagram and alkaline–tholeiitic discrimination boundary of Macdonald (1968)] retrieved from the GEOROC database. Sample selection was made to obtain the most comprehensive dataset of trace and major element analyses and is not exhaustive. All lava data were normalized by addition of olivine to reach a magma composition in equilibrium with an olivine composition of Fo_{88} . Normalizing values used are from Lyubetskaya & Korenaga (2007). Data sources for lavas from East, Possession and Penguin Islands are as in Fig. 3.

element signatures in both Penguin and East Islands (Fig. 11b), associated with the isotopic differences reported for Pb–Sr–Nd isotopes by Breton *et al.* (2013), indicates inter-island source heterogeneity at the scale of the archipelago, such as those identified in the Pacific and Atlantic Oceans (e.g. Blichert-Toft & Albarède, 2009; Rohde *et al.*, 2013).

Interestingly, the average trace element abundance patterns of basalts from the Prince Edward (Marion Island; e.g. Janney *et al.*, 2005), Kerguelen (e.g. Doucet *et al.*, 2006), Comoros (e.g. Class *et al.*, 1998) and Mascarene (e.g. Paul *et al.*, 2007) archipelagos (Fig. 11b) all exhibit the same positive Ba anomaly relative to Th and Rb, similar to that observed for Penguin Island. Although the pattern for Penguin Island shares some

similarities with that of Kerguelen picrites (Fig. 11b; Doucet *et al.*, 2006), the pattern for Kerguelen does not display a negative anomaly in K relative to Nb. This observation suggests that their mantle sources constitute two physical entities with distinct compositions. Nonetheless, a connection, rather than a separation, between the Kerguelen and Crozet tails has been imaged by seismic tomography in this region (Montelli *et al.*, 2004, 2006), but with a low lateral resolution (~ 1000 km). We cannot at present exclude the possibility that Crozet might originate as a secondary diapir of the main Kerguelen conduit emerging from the African superplume, if this structure is chemically heterogeneous. The average trace element patterns of Penguin and Prince Edward–Marion islands are also similar (Fig. 11b). However, the mantle source of Penguin Island cannot be considered as a secondary expression of that of the Prince Edward archipelago, because the Penguin Nd–Pb isotope field does not overlap with, or necessarily converge towards, the Marion–Prince Edward Nd–Pb isotope field, as reported by Breton *et al.* (2013). The same conclusion holds when the chemical attributes of Penguin Island are compared with those of the Mascarene Islands, as their Sr–Nd isotopic compositions define two distinct fields (Breton *et al.*, 2013).

Buffering of LILE by a potassic phase?

When normalized to primitive mantle, the trace element patterns of our lavas show deviations from smooth patterns in Rb, Ba, and K relative to neighboring elements, indicating the presence of a residual phase, unlike the typical anhydrous mantle assemblage in the source of the East Island lavas, which holds back these elements from the melt (Figs 5a and 11). This is further illustrated when the behavior of fractionation-corrected LILE and immobile elements are examined in diagrams such as Th/Ba versus Th (Fig. 12a). The systematics of these elements can be interpreted in term of varying degrees of equilibrium melting of a mantle source in which the proportions of minerals entering the melt and the mineralogy of the source remain fixed (Clague & Frey, 1982). The sense of curvature in such a diagram is determined by the relative magnitude of the bulk partition coefficients of the two incompatible elements involved.

If the bulk partition coefficient of Th is greater than that of Ba, as expected from progressive melting of an anhydrous lherzolite, a negatively curved array will be produced at small degrees of melting in Th/Ba versus Th space. The same holds for the systematics in Ce/K–Ce space, as the bulk partition coefficient of K should be slightly lower than that of Ce (Fig. 12b). However, in each diagram, a slight and scattered increase is observed in Th/Ba and Ce/K with increasing Th and Ce, in striking contrast to the expected overall negatively curved arrays (Fig. 12). These features are thus inconsistent with variable amounts of melting of an anhydrous lherzolite source assemblage, but reflect the

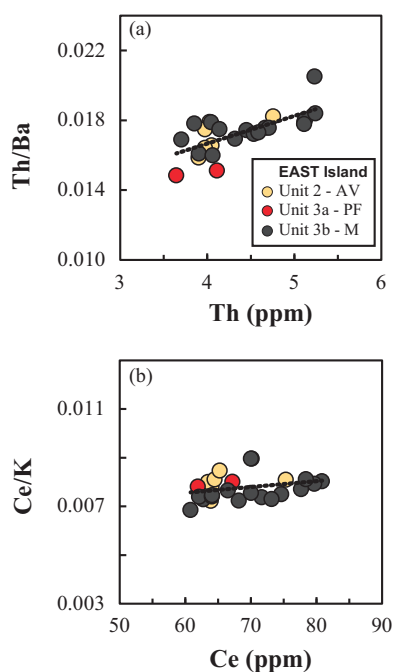


Fig. 12. Abundance ratios of incompatible elements vs concentrations of Th and Ce (ppm) for East Island samples (Crozet archipelago). (a) Th/Ba vs Th; (b) Ce/K vs Ce. AV, Albatros Valley; PF, Penguin Falls; M, Mt Marion. All lava data were normalized by addition of olivine to reach a magma composition in equilibrium with olivine of composition FO_{88} .

presence in the source of small amounts of a K-bearing hydrous residual phase, such as amphibole or phlogopite. Such phases are major hosts for Rb, Ba, K, and other LILE during early melting stages (e.g. [Class & Goldstein, 1997](#)).

Another potential candidate as a K-bearing phase is clinopyroxene, which is stable in the deep mantle at pressures of 5–15 GPa and temperatures of 1000–1500°C ([Harlow, 1997](#); [Tsuruta & Takahashi, 1998](#); [Safonov *et al.*, 2011](#)). However, we consider it unlikely that melting took place in the presence of residual K-bearing clinopyroxene as (1) near-horizontal trends of CaO versus MgO and SiO₂ are not defined by our data, and (2) the high pressures coupled with the high mantle potential temperatures required for the generation of these alkaline melts ([Tsuruta & Takahashi, 1998](#)) would generate significantly larger volumes of magmatism than are apparent on East Island.

If the presence of a hydrous K-bearing phase in the source of the East Island lavas is confirmed, any calculation of mantle potential temperature using an anhydrous mantle paragenesis will be erroneous. The same is true when melting pressures are estimated using a comparison with experimental liquids derived from anhydrous melting experiments on KR4003.

What is the nature of the K-bearing phase?

The occurrence of residual K-bearing hydrous phases is not unusual in OIB mantle sources; this has been

frequently invoked to explain the petrogenesis of a number of primitive alkaline volcanic suites from basanite to nephelinite (e.g. [Clague & Frey, 1982](#); [Halliday *et al.*, 1995](#); [Wulff-Pedersen *et al.*, 1996](#); [Class & Goldstein, 1997](#); [Reiners & Nelson, 1998](#); [Gurenko *et al.*, 2006](#); [Sisson *et al.*, 2009](#)). These phases are stable in cold geotherm environments beneath either continents or old ocean basins. Pargasitic amphibole or phlogopite are not stable phases at high temperature, and cannot survive in the convective asthenospheric mantle (e.g. [Frost, 2006](#)). The upper stability limit of pargasitic amphibole in upper mantle rocks ranges from 1 to 3 GPa at temperatures between 970 and 1170°C (e.g. [Wallace & Green, 1988](#); [Mengel & Green, 1989](#); [Niida & Green, 1999](#); [Frost, 2006](#)), whereas that of phlogopite extends to 8–9 GPa and 1100–1200°C in peridotites (e.g. [Wendlandt & Egger, 1980](#); [Konzett & Ulmer, 1999](#)), and up to 7.5 GPa and 1400°C in clinopyroxenites ([Luth, 1997](#)).

Although East Island sits on old, thick lithosphere, a contribution from residual amphibole in the mantle source of the lavas from Units 2 and 3 appears unlikely. First, the inference that garnet is a residual phase requires melting to proceed at pressures above the spinel–garnet transition (~2.8 GPa; [Robinson & Wood, 1998](#)) close to the stability limit of amphibole (~3.0 GPa). Second, melts derived from an amphibole-bearing lherzolite source will exhibit fractionation of MREE relative to HREE, forming a convex-upward pattern in the MREE because of the affinity of calcic amphiboles for the MREE (Gd to Ho) relative to the HREE (Er to Lu; [Tiepolo *et al.*, 2000, 2007](#)). The REE patterns of the East Island lavas do not have a convex ‘bump’ in the MREE (Fig. 6).

Low-degree partial melting of a phlogopite–garnet-bearing lherzolite source, leaving residual phlogopite, is considered the most likely for generating the lavas from Units 2, 3a and 3b on East Island. First, the mineral–melt partition coefficient for Sr is significantly lower for phlogopite than for amphibole (amphibole D_{Sr} 0.62; [Tiepolo *et al.*, 2007](#); phlogopite D_{Sr} 0.058; [Schmidt *et al.*, 1999](#)). Second, the partition coefficients for Ba and Rb are less contrasted in phlogopite than in amphibole, in which Ba is much more strongly partitioned than Rb ([Tiepolo *et al.*, 2007](#)). Third, the high contents of many trace elements (e.g. U, Th, Sr, and REE) in East Island lavas probably reflect the lack of partitioning of these elements in phlogopite during melting ([La Tourette *et al.*, 1995](#); [Schmidt *et al.*, 1999](#); [Adam & Green, 2006](#)).

Melting model

Modeling melt compositions derived from phlogopite-bearing mantle assemblages is very difficult, as the source melting behavior is not fully constrained. Melting experiments have not been performed over a range of P – T on the same chemical compositions and modal mineralogies in most relevant studies ([Bravo & O’Hara, 1975](#); [Mengel & Green, 1989](#); [Thibault *et al.*](#)

1992; Conceiccao & Green, 2004). No constraints for incipient melting are at present available for these lithologies. Most experimental studies of trace element partitioning in mafic alkaline magmas have been dedicated to basanite or lamproite equilibria (La Tourette *et al.*, 1995; Schmidt *et al.*, 1999; Adam & Green, 2006). With these limitations in mind, we have nevertheless chosen to test whether the average trace element composition of East Island lavas normalized to be in equilibrium with Fo₈₈ can be approximated by a simple incongruent batch melting of a phlogopite–garnet-bearing peridotite. Although not shown, pairs of elements having near-equal degrees of incompatibility (Nb–Ta, Th–U, Zr–Hf) define pseudo-linear abundance correlations in all studied units (2, 3a and 3b) of East Island, enhancing the likelihood that these units have been derived from the same source rock composition by variable degrees of partial melting. Our simple model requires many *ad hoc* selections of partition coefficients, mineral modes, and melting reactions, and therefore is susceptible to initial interpretations, potential biases, and oversights. The modal mineralogy, melt reaction stoichiometry, modelled source composition and partition coefficients are presented in Tables 4 and 5. Once the modal mineralogy, melting and partition coefficients were fixed, the trace element composition of the mantle source was iteratively estimated by adjusting its concentration and melting extent so that the melt composition matches that of the average calculated parental magma. In this way, the average trace element patterns of the East Island lavas normalized to Fo₈₈ can be broadly reproduced by non-modal batch melting of a phlogopite–garnet-bearing peridotite at an average melting degree of ~1.7% (Fig. 13). Extraction of such small melt fractions can be achieved owing to volatile-rich conditions, which cause a reduction of the viscosity and density of the melts (Wendlandt & Egger, 1980; McKenzie, 1989; Mengel & Green, 1989; Faul, 2001; Enggist *et al.*, 2012).

Our modelled source composition falls within or near the upper limit of Bulk Silicate Earth or primitive mantle estimates (Fig. 13a; e.g. Jagoutz *et al.*, 1979; Anderson, 1983; Taylor & McLennan, 1985; Hofmann, 1988; Hartmann & Wedepohl, 1993; McDonough & Sun, 1995; Palme & O'Neill, 2004; Lyubetskaya & Korenaga, 2007), except for K (900 ppm) and Rb (1.7 ppm; Table 5). As shown by the primitive mantle normalized trace element pattern of our modelled source (Fig. 13a), the presence of phlogopite in a mantle assemblage increases its K₂O, Rb and Ba contents well above most primitive mantle values (Table 5), as a result of preferential incorporation of these elements in this mineral (e.g. Gregoire *et al.*, 2000). The U-shaped trace element pattern of our modelled source, which defines a steep irregular decrease in relative concentration from Rb to Pb coupled with a slight and discontinuous increase from Pb to Y, requires that the mantle source has previously experienced at least one melting event before being re-fertilized by low-degree alkali-rich silicate

melts. This U-shaped pattern, at least for highly to moderately incompatible elements, shares similarities with those of metasomatically enriched Finero harzburgites (Hartmann & Wedepohl, 1993; Zanetti *et al.*, 1999; Fig. 13a). With the exception of Sr, we note that the trace element pattern of our modelled source also bears a strong resemblance to that determined by Sisson *et al.* (2009) for early Kilauea lavas, whose mantle source is also considered to have been previously depleted by melt extraction and subsequently metasomatically enriched (Fig. 13a). The negative Sr anomaly in our source may point to an absence of residual carbonate minerals, which is consistent with the absence of negative anomalies in Ti, Zr and Hf in our magma compositions. Finally, the requirement for phlogopite in the source suggests that the average mantle potential temperature should be much lower than predicted (~1542°C) by Putirka (2008). In addition to water, high contents of alkalis are noteworthy for depressing the mantle solidus temperature of peridotite (Hirschmann, 2000; Brey *et al.*, 2011). In particular, metasomatism by ~3–4% siliceous alkali melt could lower the peridotite solidus by 100°C or more (Hirschmann, 2000).

How is phlogopite formed?

The signature of phlogopite in the mantle source of East Island lavas points to a style of metasomatism that has been well described in subcontinental and/or sub-arc regions (Rogers *et al.*, 1992; Foley *et al.*, 1999; Le Roex *et al.*, 2003; Maria & Luhr, 2008), and to a lesser extent in oceanic environments. In subduction settings phlogopite forms and stabilizes in the mantle wedge through reactions of K-rich hydrous fluids arising from the breakdown or melting of the white mica phengite in the subducting lithosphere (Eggins *et al.*, 1998; Konzett & Ulmer, 1999; Schmidt *et al.*, 2004; Hermann & Spandler, 2008). Some fossilized mantle wedges, such as the Horoman, Ulten and Finero ultramafic complexes, have been affected by potassic metasomatism before exhumation to the surface (Yoshikawa *et al.*, 1993; Brandon *et al.*, 1999; Zanetti *et al.*, 1999, 2013; Scambelluri *et al.*, 2006). These K-rich mantle domains are generated by LILE transfer into the overlying mantle wedge either by high-pressure, hydrous, siliceous, potassic trondhjemitic to granitic melts derived from sediment melting at pressures greater than 4 GPa or by supercritical fluids derived from the oceanic crust above 6.5 GPa (Schmidt *et al.*, 2004; Hermann & Spandler, 2008).

In cratonic mantle xenoliths progressive modal metasomatism, involving the precipitation of phlogopite, clinopyroxene and spinel at the expense of garnet and orthopyroxene, can lead to refertilization of refractory harzburgites into lherzolite or wehrlite (Van Ackerbergh *et al.*, 2001). Melt–harzburgite interactions, with precipitation of clinopyroxene and phlogopite at the expense of olivine and orthopyroxene, have also been experimentally reproduced by Thibault *et al.*

Table 4. Partition coefficients, mineralogical mode and melting reaction

Phase	Mode	Melting reaction	Partition coefficients ($K_{d_{\text{mineral/melt}}}$)														
			K	Ti	Sr	U	Th	Pb	Rb	Ba	Nb	Zr	Hf	La	Ce	Nd	Y
Olivine	0.57	-0.171	0.0001 ^a	0.006 ^a	0.00004 ^b	0.0013 ^c	0.000014 ^d	0.0035 ^c	0.0003 ^b	0.0011 ^c	0.000041 ^e	0.0013 ^e	0.005 ^e	0.0004 ^a	0.00006 ^e	0.003 ^f	0.007 ^e
Clinopyroxene	0.12	0.500	0.047 ^g	0.1 ^a	0.103 ⁱ	0.003 ^c	0.014 ^h	0.011 ⁱ	0.0019 ^g	0.02 ^f	0.0048 ^h	0.053 ^c	0.081 ^c	0.0289 ^g	0.0446 ^g	0.0916 ^g	0.2558 ^g
Orthopyroxene	0.232	-0.057	0.0039 ^j	0.086 ^b	0.0021 ^f	0.0078 ^c	0.0086 ^c	0.0091 ^c	0.0038 ^f	0.0036 ^f	0.002 ^h	0.036 ^h	0.046 ^c	0.00041 ^g	0.00101 ^g	0.00268 ^g	0.085 ^c
Garnet	0.060	0.114	0.22 ^j	0.1 ^a	0.0017 ^k	0.037 ^c	0.009 ^c	0.0054 ^c	0.002 ^f	0.0007 ^c	0.00054 ^k	0.381 ^c	0.369 ^c	0.0017 ^g	0.0058 ^g	0.0495 ^g	1.84 ^g
Phlogopite	0.018	0.614	8.5 ^l	0.71 ^f	0.058 ^m	0.00006 ^m	0.000005 ^m	0.2164 ⁿ	6.41 ^o	5.24 ⁿ	0.021 ^k	0.012 ^f	0.015 ^f	0.0004 ^f	0.0003 ^f	0.0009 ^f	0.003 ^f

^aHawkesworth *et al.* (1993). ^bHalliday *et al.* (1995). ^cSalters *et al.* (2002). ^dMcDade *et al.* (2003). ^eDonnelly *et al.* (2004). ^fAdam & Green (2006). ^gPartition coefficients for REE, K and Rb between liquid, clinopyroxene and garnet were recalculated using lattice-strain models (Wood & Blundy, 1997; Draper & Van Westrenen, 2007) and mineral-liquid compositions produced by experimental melting at high pressure (Salters *et al.*, 2002). ^hSalters & Longhi (1999). ⁱNiu *et al.* (1999). ^jVan Westrenen *et al.* (1999). ^kGreen *et al.* (2000). ^lThe partition coefficient used for K between liquid and phlogopite falls in the range 12–12 as shown by Green (1994). ^mSchmidt *et al.* (1994). ⁿGregoire *et al.* (2000). ^oFoley *et al.* (1996). The melting reaction coefficients are derived from the 3 GPa phlogopite lherzolite melting experiment of Thibault *et al.* (1992).

Table 5. Inferred mantle source trace element composition compared with primitive mantle composition estimations

K	Ti	Sr	U	Th	Pb	Rb	Ba	Nb	Zr	Hf	La	Ce	Nd	Y	Reference
<i>Modelled source</i>															
900	947	13.5	0.023	0.094	0.053	1.7	15	0.71	11.0	0.3	0.69	1.60	1.12	4.1	This study
<i>Primitive mantle</i>															
240	1205	19.9	0.0203	0.0795	0.15	0.60	6.6	0.66	10.5	0.283	0.648	1.675	1.25	4.3	McDonough & Sun (1995)
151	1225	16.2	0.0196	0.0765	0.12	0.39	5.22	0.97	13.0	0.330	0.57	1.40	1.02	3.26	Anderson (1983)
183	959	17.8	—	0.064	—	0.55	5.1	0.56	8.3	0.270	0.551	1.436	1.067	3.4	Taylor & McLennan (1985)
260	1280	20.3	0.0218	0.0834	0.185	0.61	6.75	0.588	10.81	0.3	0.686	1.786	1.327	4.37	Palme & O'Neill (2004)
258.2	1085	18.21	0.0203	0.0813	0.175	0.5353	6.049	0.6175	9.714	0.2676	0.6139	1.6011	1.1892	3.940	Hofmann (1988)
190	947	15.8	0.0173	0.0626	0.144	0.457	5.08	0.46	8.42	0.227	0.508	1.34	0.994	3.37	Lyubetskaya & Korenaga (2007)
260	1300	28	0.0260	0.094	—	0.81	6.9	0.90	11.0	0.35	0.63	—	—	4.6	Jagoutz <i>et al.</i> (1979)
450	743	11.4	0.0360	0.180	—	1.50	17.9	0.44	10.0	0.260	0.76	1.40	1.10	3.6	Hartmann & Wedepohl (1993)
250	1300	21.1	0.0021	0.085	0.185	0.635	6.989	0.713	11.2	0.309	0.687	1.775	1.354	4.55	Sun & McDonough (1989)

(1992). This style of metasomatism, recording interaction of the lithosphere with asthenospheric melts, is extensive in Southern Africa, where the mineralogical and chemical characteristics of metasomatized mantle xenolith melts point towards a silicate melt of broadly alkaline character (Van Achterbergh *et al.*, 2001; O'Reilly & Griffin, 2013) as the metasomatizing agent.

In intraplate oceanic settings, the distribution of residual phlogopite in mantle sources seems to be associated with the presence of a thick and/or old lithosphere (e.g. Comoros, Hawaii, Canary Islands; Clague & Frey, 1982; Wulff-Pedersen *et al.*, 1996; Class *et al.*, 1998; Geldmacher & Hoernle, 2000; Doucelance *et al.*, 2003; Gurenko *et al.*, 2006; Prægel & Holm, 2006; Sisson *et al.*, 2009; Van Der Zander *et al.*, 2010), because of its cooler geotherm, roughly equivalent to that of continental areas (Stein, 1995). At Hawaii, the compositions of some lavas from Niihau, Oahu and early Kilauea can be accounted for by variable degrees of partial melting of a phlogopite–garnet-bearing peridotite (Clague & Frey, 1982; Dixon *et al.*, 2008; Sisson *et al.*, 2009). The phlogopite might have been inherited from previous silicate and/or carbonatite metasomatism of previously depleted peridotite. Both at Comoros (La Grille) and the Canary Islands, where the lithosphere is thick, the trace element characteristics of the alkaline lavas point to the presence of phlogopite and/or amphibole in the mantle source (Hoernle & Schmincke, 1993; Class & Goldstein, 1997; Class *et al.*, 1998). Phlogopite and amphibole fingerprints observed in lavas from the Canary Islands have been interpreted as ghost signatures carried by upward mantle plume flow containing 'amphibole-' or 'phlogopite/phengite-exhausted' recycled oceanic crust (Gurenko *et al.*, 2006).

As observed at Hawaii and the Canary Islands, the modelled trace element attributes of the East Island mantle source indicate the presence of metasomatized lithospheric mantle, through which an alkali-rich silicate melt has percolated and metasomatically overprinted pre-existing depleted mantle wall-rocks. Although carbonatite metasomatism has been recognized in the mantle sources of lavas from Hawaii (e.g. Dixon *et al.*, 2008; Sisson *et al.*, 2009), Cape Verde, and the Canary

Islands (e.g. Hoernle *et al.*, 2002), all associated with old, thick, oceanic crust (≥ 100 Ma), our data for East Island do not provide any evidence for a carbonatitic character of the metasomatic melt. The trace element pattern of our modelled source lacks the typical strong negative anomalies in Zr, Hf and Ti relative to Y (Fig. 13a) commonly observed in oceanic carbonatites (e.g. Hoernle *et al.*, 2002; Bizimis *et al.*, 2003). The latter systematically show marked depletions in Rb, K, Zr, Hf and Ti and enrichments in Ba, Th, LREE, MREE, Pb and Sr when compared with silicate rocks from oceanic islands (e.g. Hoernle *et al.*, 2002). Instead, the high average ratios of Th/Nb (0.11 ± 0.02) and Th/Ta (1.68 ± 0.31) of our East Island suite might reflect a sediment fingerprint in the mantle source, as high Th (i.e. high Th/Nb) contents in arc lavas commonly reflect sediment melting (Elliott *et al.*, 1997; Johnson & Plank, 1999).

Dynamic model

Beneath a near-stationary plate, a rising mantle plume should spread nearly radially symmetrically at the lithosphere–asthenosphere boundary (Agrusta *et al.*, 2013). Its melting regime can be approximated either as a cylinder (conduit) or a sphere (plume head). After melt extraction, decompression melting will leave a mantle residue, the depletion of which varies both horizontally and vertically (Arndt *et al.*, 2002, 2009). Because of decreasing temperature from the plume conduit centre to its margins, the solid residue gradually evolves from a refractory harzburgitic, low-density material in the core to a denser, less-depleted peridotite in the outer sheath (Arndt *et al.*, 2002, 2009). Because of increasing extent of melting upwards, the residual mantle column shows increasing depletion upwards.

As the rate at which the residual mantle is replenished by plume melting directly depends on lithosphere thickness and on how fast material can spread laterally away from the plume source (Phipps Morgan *et al.*, 1995), it is unlikely that beneath East Island the depleted core is dragged far away from the melting locus because of near-stationary plate motion (~ 6.46 mm a⁻¹; King & Adam, 2014), thick lithosphere and ultraslow plume upwelling (≤ 2 cm a⁻¹; Bourdon *et al.*, 2006) as

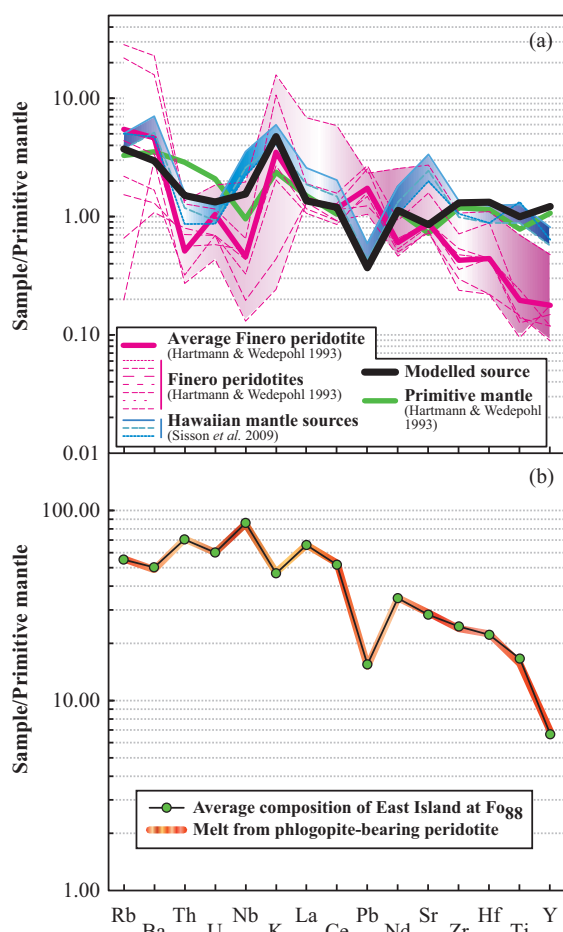


Fig. 13. Primitive mantle normalized trace element patterns of modelled source, melt and average composition of East Island basalts normalized to $F_{0.88}$. Primitive-mantle values are from Lyubetskaya & Korenaga (2007). (a) Primitive mantle trace element abundances estimated for the modelled source of the East Island suite compared with the composition of Finero peridotites (Hartmann & Wedepohl, 1993), modelled source compositions of early Kilauea lavas (Sisson *et al.* 2009) and primitive-mantle composition estimation of Hartmann & Wedepohl (1993). The pink field denotes the compositional range of Finero peridotites (Hartmann & Wedepohl, 1993), whereas the blue field shows theoretical source compositions for early Kilauea lavas (Sisson *et al.*, 2009). The thick green curve corresponds to the primitive-mantle composition estimation of Hartmann & Wedepohl (1993). (b) Averaged fractionation-corrected primitive mantle normalized incompatible element patterns of East Island samples compared with that of a modelled low-degree melt ($\sim 1.7\%$) produced by non-modal equilibrium melting of a phlogopite-garnet-bearing peridotite.

inferred from its low buoyancy flux ($0.25\text{--}0.5\text{ Mg s}^{-1}$; Sleep, 1990; King & Adam, 2014). Residual mantle accumulation may be further favored as the lithosphere beneath Crozet might be thicker than predicted by a simple half-space square root of time lithosphere cooling model ($\sim 86\text{ km}$; Parsons & Sclater, 1977; Phipps Morgan & Smith, 1992; Stein & Stein, 1992), because weaker plumes cool more than stronger plumes as they ascend (Albers & Christensen, 1996). With aging, such a depleted root will also thicken (Phipps Morgan *et al.*, 1995), reducing the amount of near-plume melting. In

addition, because of the extremely slow replenishment of the melting regime by plume flow and because of the strong melting localization, one would expect that the residual material spends more time in the melting regime than for stronger plumes. Therefore, the proportion of refractory (harzburgite) versus fertile material (Iherzolite) should increase with time in the central region produced upon melting.

Indeed, numerical modelling for a plume head making contact with a stationary thick plate predicts the formation of a depleted root and its progressive thickening with time above the plume core (Manglik & Christensen, 1997), owing to its resistance to downward advection away from the plume axis. During the early formation of the root (up to 6–15 Ma), the narrowing and speeding up of the upwelling induced by the density change caused by Fe depletion is accompanied by an increase of the melt production rate (Manglik & Christensen, 1997). After 6–15 Myr, the stagnation of the plume flow at greater depth in response to progressive accumulation of the depleted root is associated with a decrease in melt production rate. During this latter period, the lithosphere-like layer might become destabilized away from the plume (at 100–200 km distance) with the development of small-scale lithospheric instabilities (Manglik & Christensen, 1997). The thermal structure becomes unstable because cold, high-density material is perched above hot, lower density mantle and because it takes too long for residual material to be transported from the center to the walls of the melting regime. However, if considering a wet melting regime, an increase of the viscosity of the residue caused by volatile loss during melting might potentially suppress small-scale instabilities, enhancing the resistance against convective removal of the residue from the top of the plume (Manglik & Christensen, 1997) in response to lower upwelling rate.

Although the downward component in this system was not modelled by Manglik & Christensen (1997), one can ask the question whether the periodic sinking of instabilities in the re-fertilizing mantle periodically increases upwelling velocity and melting rate, which would account for the time-varying fluctuations in melt production rate after 6–15 Myr predicted by their model. Another issue is whether metasomatic processes are enhanced at the top of the melting regime during the weak melt generation period, once the harzburgitic root has begun its growth. During this latter phase, one might also argue that a progressive local closure of the central melting regime might gradually cause the upwelling to deviate, leading to a displacement of the melting locus (Phipps Morgan *et al.*, 1995; Manglik & Christensen, 1997).

The extent to which metasomatic processes during weak melt production periods might re-fertilize the depleted lithospheric root is difficult to determine, as it is strongly dependent on previous episodes of mantle depletion, the extent of melt impregnation (e.g. melt/rock ratio) of the depleted mantle wall-rock and the

degree of enrichment of the metasomatic melt. If the residue has been extensively depleted by one or more melting events, its re-fertilization by low-degree melts is expected to easily overprint its ultra-depleted trace element signature. Its degree of Fe depletion will depend on the Fe depletion of the initial residue and the Fe enrichment of the metasomatic melt, both governed by the melting pressure and the melting extents at which they were generated, and the proportion of metasomatizing melt added. Melting of a refractory source shifts melt compositions towards higher MgO and FeO concentrations relative to those derived from a more fertile source (e.g. Falloon & Danyushevsky, 2000; Parman & Grove, 2004). So perhaps, in this latter case, even if the Fe content of the residue is increased by metasomatic addition, a very slight increase in Fe content of the aggregated lavas to levels greater than those of normal mantle might be preserved. However, Fe enrichment is not obvious in East Island lavas. Similarly, it is difficult to predict how buoyant the residual metasomatized mantle will be, as the effects of Fe depletion in olivine and orthopyroxene will be counterbalanced by changes in the modal proportion of garnet, olivine, orthopyroxene, phlogopite and clinopyroxene (Thibault *et al.*, 1992; Van Achterbergh *et al.*, 2001) induced by harzburgite–melt interactions. Both parameters affect the mantle density (Schutt & Leshner, 2006). The seismic detection of such metasomatized residues is challenging, as in addition to the metasomatism-induced perturbation of the seismic signal, previous melt depletion in the garnet stability field is not predicted to cause significant seismic velocity variations (<2%; Schutt & Leshner, 2006; Afonso & Schutt, 2012). In summary, the presence of such remnants in the mantle source or at the base of the lithosphere will leave few obvious geochemical and geophysical traces, except perhaps some light signatures in Fe isotopes (Williams & Bizimis, 2014).

As mentioned above, evidence for melting of residual mantle beneath East Island is provided by the approximately U-shaped trace element pattern of the modelled source. This U-shaped pattern has strong similarities to those of the metasomatized depleted mantle sources of Finero (Hartmann & Wedepohl, 1993) and early Kilauea lavas (Sisson *et al.*, 2009). Such patterns require that the mantle source has previously experienced one or more melting events before being re-fertilized by low-degree alkali-rich silicate melts. According to the numerical modelling of Manglik & Christensen (1997), we thus speculate that the East Island lavas reflect melting of the metasomatized depleted root once it had already significantly thickened, forcing melting termination to higher pressures and a reduced mean melting extent. Indeed, the first magmatic unit of East Island is dated at ~8.75 Ma, whereas the second and third units from which our samples were obtained range in age from 0.9 to 0.4 Ma, based on K–Ar geochronology (Chevallier *et al.*, 1983; Verwoerd *et al.*, 1990). As the depleted root

grows, an even colder thermal lithosphere environment probably develops owing to enhanced conductive processes related to its growing thickness and weak plume buoyancy, which might favor metasomatic processes at its base. Under conditions of ultraslow ascent, the mantle plume melts by decompression when crossing the lherzolite solidus. Alkali-rich low-degree silicate melts are released, migrate upward, impregnate the overlying depleted harzburgitic root and solidify, refertilizing it in clinopyroxene and phlogopite. Once the root geotherm is subsequently raised (by increased heat supply from the plume either by conductive heating or from subsequent percolating melts), preferential melting of these refertilized peridotites relative to the depleted refractory harzburgitic portions might occur. The construction of the depleted root might also be responsible for the horseshoe-shaped spatial distribution of oceanic islands at Crozet and the extreme height of its topographic bulge (1543–1756 m; Monnereau & Cazenave, 1990; King & Adam, 2014).

Mantle melting residues floating above normal asthenosphere are expected to be more abundant in environments in which lateral mantle flow is slowed down by slow upwelling, slow absolute plate motions or physical barriers such as transform faults or propagating rift configurations. Such residues may have preferentially accumulated in the Southern Indian Ocean mantle in response to slow Antarctic plate motions since ~30 Ma. Evidence for the presence of refractory components in mantle sources of the easternmost ultraslow Southwest Indian Ridge and Australian–Antarctic Discordance, characterized by ultraslow upwelling and/or propagating rifts, has been provided by the depletions in Ti and moderately incompatible elements observed in their erupted basalts (e.g. Klein *et al.*, 1991; Meyzen *et al.*, 2003). Whether such mantle residues remain at shallow levels or sink into the mantle will depend on the competition between their abundances and chemical buoyancies, the efficiency of mantle convection and plate motion forces (Dupeyrat *et al.*, 1995). At slow plate velocities, sinking of the residual mantle portions is rather unlikely over short time scales. Faster plate motions will more easily force chemically buoyant material down into the deeper mantle (Dupeyrat *et al.*, 1995).

We note that our proposed model for the formation of depleted roots below ocean islands atop motionless plates bears strong similarities to that proposed by Arndt *et al.* (2002, 2009) for cratonic keel genesis. According to those researchers, the residue left after melt extraction in a cylindrical melting regime is vertically and horizontally stratified from dense, more fertile mantle in the outer sheath and towards the base of the melting zone, to refractory, low-density mantle in the uppermost core of the melting zone. The latter material would gradually accumulate as the plume nears the surface, whereas the denser, more fertile parts of the plume would be ejected by gravitational redistribution.

Keels are thus built from an accumulation of melt residues derived from plume melting.

In conclusion, the exploration of magmatic processes at oceanic islands on motionless plates should have wide-ranging implications for furthering our understanding of the early and modern evolution of magmatic processes at intraplate settings on Earth and of the inner planetary workings of volcanic systems on other planets, which do not have a present-day plate-tectonic regime (e.g. Mars; Meyzen *et al.*, 2015). To date, to model the evolution of chemical heterogeneities in planetary mantles, most workers have assumed that mantle heterogeneities are simply displaced in the melting regime and vanish. However, future studies should include the effect of the buoyancy of the depleted mantle on the rate of melting and on the geometry of mantle plume flow.

CONCLUSIONS

Combined trace and major element systematics in Quaternary lavas (Units 2, 3a and 3b) from the easternmost and oldest island of the Crozet archipelago, East Island, suggest a complex multi-stage dynamic evolution of their mantle source, controlled by some of the lowest-velocity mantle flow patterns found among Earth's intraplate melting regimes. The trace element signature of these lavas requires that some pre-existing, residual depleted mantle has been metasomatically enriched by percolating alkali-rich silicate melts, leaving a garnet–phlogopite-bearing peridotite source. Melting at an average degree of $\sim 1.7\%$ of such a lithospheric mantle source accounts for the mean trace element composition of East Island lavas. The pre-existing depleted mantle component may be composed of residues left behind by previous melting events that have not been dragged away from the melting locus. Low-degree alkali-rich melts, which metasomatize the depleted root, can be derived from the fertile plume source. As the plume is continually rising at the lithosphere–asthenosphere boundary at an extremely slow rate, low-degree melts are released, which migrate upward, resolidify and react with the overlying depleted root, refertilizing it in clinopyroxene and phlogopite. Over time, long-term heating and decompression caused by the underlying plume lead to the preferential melting of these refertilized peridotites relative to the harzburgitic residues. In melting regimes associated with low-velocity mantle flow fields, the repeated transit of alkali magmas through the lithosphere could lead to chemical modification and subsequent melting of thick, cold oceanic lithospheric mantle. Such processes might be relevant to all terrestrial and extra-terrestrial melting environments, where the lateral component flows of the melting regime are slowed down (e.g. ultraslow-spreading ridges and propagating rifts).

At the scale of the archipelago, the systematics of trace elements between the eastern (East and Possession Islands) and western (Apostles Islets, and

Penguin and Pig Islands) groups provide evidence for a change in mantle source composition. The trace element compositions of lavas from East and Possession Islands (Breton *et al.*, 2013) are similar, suggesting that they were derived from the activity of the same volcanic system for more than ~ 8 Myr. They do not resemble those of the Reunion shield volcanoes, and differ markedly from those of the nearby Marion hotspot and distant Kerguelen archipelago. In contrast, the trace element composition of Penguin Island lavas is distinct from those of East and Possession Islands, which suggests an inter-island source heterogeneity at the scale of the archipelago, such as those identified in the Pacific and Atlantic Oceans (e.g. Blichert-Toft & Albarède, 2009; Rohde *et al.*, 2013).

ACKNOWLEDGEMENTS

This work is dedicated to the memory of Professor John Mahoney. We are deeply grateful to Jacques Nougier for his contribution to the early stages of this project; Steve Carey for providing the core samples for this study; Charles Knaack for the inductively coupled plasma mass spectrometry analyses; Giancarlo Cavazzini for access to the chemical facilities at Padua University; and Matteo Massironi, Douglas Pyle, and Daniel Sauter for assistance and extensive discussions. Janne Blichert-Toft and Joanne Whittaker are thanked for insightful and invaluable comments on an earlier version of this paper. Michael Bizimis and Cornelia Class are thanked for their detailed and thoughtful reviews, which greatly improved this paper. We also thank Simon Turner for editorial handling.

FUNDING

This work was supported by a grant of the National Science Foundation (grant number OCE-644625) for the curation of geological samples at the University of Rhode Island, a grant of the University of Padua (grant number ATENEO CPDA114007/11) to C.M.M. and a grant of the Cassa di Risparmio di Padova e Rovigo (grant number MARZECCE08) to A.M.

SUPPLEMENTARY DATA

Supplementary data for this paper are available at *Journal of Petrology* online.

REFERENCES

- Adam, J. & Green, T. (2006). Trace element partitioning between mica- and amphibole-bearing garnet lherzolite and hydrous basanitic melt: 1. Experimental results and the investigation of controls on partitioning behaviour. *Contributions to Mineralogy and Petrology* **152**, 1–17.
- Afonso, J. C. & Schutt, D. L. (2012). The effects of polybaric partial melting on density and seismic velocities of mantle restites. *Lithos* **134–135**, 289–303.

- Agrusta, R., Arcay, D., Tommasi, A., Davaille, A., Ribe, N. M. & Gerya, T. (2013). Small-scale convection in a plume-fed low-viscosity layer beneath a moving plate. *Geophysical Journal International* **194**, 591–610.
- Albarède, F., Luais, B., Fitton, G., Semet, M., Kaminski, E., Upton, B. G. J., Bachelery, P. & Cheminée, J.-L. (1997). The geochemical regimes of Piton de la Fournaise volcano (Reunion) during the last 530 000 years. *Journal of Petrology* **38**, 171–201.
- Albers, M. & Christensen, U. R. (1996). The excess temperature of plumes rising from the core–mantle boundary. *Geophysical Research Letter* **23**, 3567–3570.
- Allègre, C. J. & Turcotte, D. L. (1986). Implications of a two component marble-cake mantle. *Nature* **323**, 123–127.
- Amelung, F. & Day, S. (2002). InSAR observations of the 1995 Fogo, Cape Verde, eruption: implications for the effects of collapse events upon island volcanoes. *Geophysical Research Letters* **29**, 1606.
- Andersen, M. B., Elliott, T., Freymuth, H., Sims, K. W. W., Niu, Y. & Kelley, K. A. (2015). The terrestrial uranium isotope cycle. *Nature* **517**, 356–359.
- Anderson, D. (1983). Chemical composition of the mantle. *Journal of Geophysical Research* **88**, 41–52.
- Argus, D. F., Gordon, R. G. & DeMets, C. (2011). Geologically current motion of 56 plates relative to the no-net-rotation reference frame. *Geochemistry, Geophysics, Geosystems* **12**, Q11001.
- Ariskin, A. A., Frenkel, M. Y., Barmina, G. S. & Nielsen, R. (1993). COMAGMAT: A FORTRAN program to model magma differentiation processes. *Computers and Geosciences* **19**, 1155–1170.
- Arndt, N., Lewin, E. & Albarède, F. (2002). Strange partners: formation and survival of continental crust and lithospheric mantle. In: Fowler, C. M. R., Ebinger, C. J. & Hawkesworth, C. J. (eds) *The Early Earth: Physical, Chemical and Biological Development*. Geological Society, London, *Special Publications* **200**, 91–103.
- Arndt, N., Coltice, N., Helmstaedt, H. & Gregoire, M. (2009). Origin of Archean subcontinental lithospheric mantle: some petrological constraints. *Lithos* **109**, 61–71.
- Beard, J. S., Lofgren, G. E., Krishna Sinha, A. & Tollo, R. P. (1994). Partial melting of apatite-bearing charnockite, granulite, and diorite: melt compositions, restite mineralogy, and petrologic implications. *Journal of Geophysical Research* **99**, 21591–21603.
- Becker, J. J., Sandwell, D. T., Smith, W. H. F., Braud, J., Binder, B., Depner, J., Fabre, D., Factor, J., Ingalls, S., Kim, S.-H., Ladner, R., Marks, K., Nelson, S., Pharaoh, A., Trimmer, R., Von Rosenberg, J., Wallace, G. & Weatherall, P. (2009). Global bathymetry and elevation data at 30 arc seconds resolution: SRTM30_PLUS. *Marine Geodesy* **32**, 355–371.
- Bellair, P. (1963). Niveaux marins anciens aux îles Crozet et Kerguelen. *Comptes Rendus de l'Académie des Sciences* **256**, 2643–2645.
- Bizimis, M., Salters, V. & Dawson, J. (2003). The brevity of carbonatite sources in the mantle: evidence from Hf isotopes. *Contribution to Mineralogy and Petrology* **145**, 281–300.
- Bizimis, M., Gautam, S., Salters, V. & Keshav, S. (2005). Hf–Nd–Sr isotope systematics of garnet pyroxenites from Salt Lake Crater, Oahu, Hawaii: evidence for a depleted component in Hawaiian volcanism. *Geochimica et Cosmochimica Acta* **69**, 2629–2646.
- Bizimis, M., Salters, V. J. M., Garcia, M. O. & Norman, M. D. (2013). The composition and distribution of the rejuvenated component across the Hawaiian plume: Hf–Nd–Sr–Pb isotope systematics of Kaula lavas and pyroxenite xenoliths. *Geochemistry, Geophysics, Geosystems* **14**, doi:10.1002/ggge.20250.
- Blichert-Toft, J. & Albarède, F. (2009). Mixing of isotopic heterogeneities in the Mauna Kea plume conduit. *Earth and Planetary Science Letters* **282**, 190–200.
- Bourdon, B., Ribe, N. M., Stracke, A., Saal, A. E. & Turner, S. P. (2006). Insights into the dynamics of mantle plumes from uranium-series geochemistry. *Nature* **444**, 713–717.
- Brandon, A. D., Becker, H., Carlson, R. W. & Shirey, S. B. (1999). Isotopic constraints on time scales and mechanisms of slab material transport in the mantle wedge: evidence from the Simcoe mantle xenoliths, Washington, USA. *Chemical Geology* **160**, 387–407.
- Bravo, M. S. & O'Hara, M. J. (1975). Partial melting of phlogopite-bearing synthetic spinel- and garnet-lherzolites. *Physics and Chemistry of the Earth* **9**, 845–854.
- Brearley, M. & Scarfe, C. M. (1986). Dissolution rates of upper mantle minerals in an alkali basalt melt at high pressure: an experimental study and implications for ultramafic xenolith survival. *Journal of Petrology* **27**, 1137–1182.
- Breton, T., Pichat, S., Moine, B., Moreira, M., Rose-Koga, E. F., Auclair, D., Bosq, C. & Wavrant, L.-M. (2013). Geochemical heterogeneities within the Crozet hotspot. *Earth and Planetary Science Letters* **376**, 126–136.
- Brey, G. P., Bulatov, V. K. & Gurnis, A. V. (2011). Melting of K-rich carbonated peridotite at 6–10 GPa and the stability of K-phases in the upper mantle. *Chemical Geology* **281**, 333–342.
- Bryan, W. B., Finger, L. W. & Chayes, F. (1969). Estimating proportions in petrographic mixing equations by least-squares approximation. *Science* **163**, 926–927.
- Chevallier, L., Nougier, J. & Cantagrel, J. M. (1983). Volcanology of Possession Island, Crozet Archipelago. In: Oliver, R. L., Jago, J. B. & James P. R. (eds) *Antarctic Earth Science*. New York: Cambridge University Press, pp. 652–658.
- Clague, D. A. & Frey, F. A. (1982). Petrology and trace element geochemistry of the Honolulu Volcanics, Oahu; implications for the oceanic mantle below Hawaii. *Journal of Petrology* **23**, 447–504.
- Class, C. & Goldstein, S. L. (1997). Plume–lithosphere interactions in the ocean basins: constraints from the source mineralogy. *Earth and Planetary Science Letters* **150**, 245–260.
- Class, C., Goldstein, S. L., Altherr, R. & Bachelery, P. (1998). The process of plume–lithosphere interaction in the ocean basins: the case of Grande Comore. *Journal of Petrology* **39**, 881–903.
- Conceicao, R. V. & Green, D. H. (2004). Derivation of potassic (shoshonitic) magmas by decompression melting of phlogopite + pargasite lherzolite. *Lithos* **72**, 209–229.
- Cottrell, E. & Kelley, K. A. (2011). The oxidation state of Fe in MORB glasses and the oxygen fugacity of the upper mantle. *Earth and Planetary Science Letters* **305**, 270–282.
- Courtney, R. & Recq, M. (1986). Anomalous heat flow near the Crozet Plateau and mantle convection. *Earth and Planetary Science Letters* **79**, 373–384.
- Crosby, A. G., McKenzie, D. & Sclater, J. G. (2006). The relationship between depth, age and gravity in the oceans. *Geophysical Journal International* **166**, 553–573.
- Damasceno, D., Scoates, J. S., Weiss, D., Frey, F. A. & Giret, A. (2002). Mineral chemistry of mildly alkalic basalts from the 25 Ma Mont Crozier section, Kerguelen archipelago: Constraints on phenocryst crystallization environments. *Journal of Petrology* **43**, 1389–1413.
- Danyushevsky, L. V. & Plechov, P. (2011). Petrolog3: integrated software for modeling crystallization processes. *Geochemistry, Geophysics, Geosystems* **12**, Q07021.

- Dasgupta, R., Jackson, M. G. & Lee, C.-T. A. (2010). Major element chemistry of ocean island basalts—conditions of mantle melting and heterogeneity of mantle source. *Earth and Planetary Science Letters* **289**, 377–392.
- DeMetz, C., Gordon, R. G., Argus, D. F. & Stein, C. (1990). Current plate motion. *Geophysical Journal International* **101**, 425–478.
- Dixon, J., Clague, D. A., Cousens, B., Monsalve, M. L. & Uhl, J. (2008). Carbonatite and silicate melt metasomatism of the mantle surrounding the Hawaiian plume: evidence from volatiles, trace elements, and radiogenic isotopes in rejuvenated stage lavas from Niihau, Hawaii. *Geochemistry, Geophysics, Geosystems* **9**, Q09005.
- Donnelly, K., Goldstein, S., Langmuir, C. & Spiegelman, M. (2004). Origin of enriched ocean ridge basalts and implications for mantle dynamics. *Earth and Planetary Science Letters* **226**, 347–366.
- Doucelance, R., Escrig, S., Moreira, M., Garipey, C. & Kurz, M. D. (2003). Pb–Sr–He isotope and trace element geochemistry of the Cape Verde Archipelago. *Geochimica et Cosmochimica Acta* **67**, 3717–3733.
- Doucet, S., Moreira, M., Weis, D., Scoates, J. S., Giret, A. & Allègre, C. (2006). Primitive neon and helium isotopic compositions of high-MgO basalts from the Kerguelen Archipelago, Indian Ocean. *Earth and Planetary Science Letters* **241**, 65–79.
- Draper, D. S. & Van Westrenen, W. (2007). Quantifying garnet–melt trace element partitioning using lattice-strain theory: assessment of statistically significant controls and a new predictive model. *Contributions to Mineralogy and Petrology* **154**, 731–746.
- Dupeyrat, L., Sotin, C. & Parmentier, E. M. (1995). Thermal and chemical convection in planetary mantles. *Journal of Geophysical Research* **100**, 497–520.
- Eggs, S. M., Rudnick, R. L. & McDonough, W. F. (1998). The composition of peridotites and their minerals. *Earth and Planetary Science Letters* **154**, 53–71.
- Elliott, T., Plank, T., Zindler, A., White, W. M. & Bourdon, B. (1997). Element transport from slab to volcanic front at the Mariana arc. *Journal of Geophysical Research* **102**, 14991–15019.
- Eggist, A., Chu, L. & Luth, R. W. (2012). Phase relations of phlogopite with magnesite from 4 to 8 GPa. *Contributions to Mineralogy and Petrology* **163**, 467–481.
- Erdmann, S., Scaillet, B. & Kellett, D. A. (2010). Xenocryst assimilation and formation of peritectic crystals during magma contamination: an experimental study. *Journal of Volcanology and Geothermal Research* **198**, 355–367.
- Falloon, T. J. & Danyushevsky, L. V. (2000). Melting of refractory mantle at 1.5, 2 and 2.5 GPa under anhydrous and H₂O-undersaturated conditions: implications for the petrogenesis of high-Ca boninites and influence of subduction components on mantle melting. *Journal of Petrology* **41**, 257–283.
- Faul, U. H. (2001). Melt retention and segregation beneath mid-ocean ridges. *Nature* **410**, 920–923.
- Foley, S. F., Jackson, S. E., Fryer, B. J., Greenough, J. D. & Jenner, G. A. (1996). Trace element partition coefficients for clinopyroxene and phlogopite in an alkaline lamprophyre from Newfoundland by LAM-ICP-MS. *Geochimica et Cosmochimica Acta* **60**, 629–638.
- Foley, S. F., Musselwhite, D. S. & Van Der Laan, S. R. (1999). Melt compositions from ultramafic vein assemblages in the lithospheric mantle: a comparison of cratonic and non-cratonic settings. In: Gurney, J. J., Gurney, J. L., Pascoe, M. D. & Richardson, S. H. (eds) *Proceedings of the Vllth International Kimberlite Conference*. Cape Town: Red Roof Design, pp. 238–246.
- France, L., Koepke, J., Ildefonse, B., Cichy, S. B. & Deschamps, F. (2010). Hydrous partial melting in the sheeted dike complex at fast spreading ridges: experimental and natural observations. *Contributions to Mineralogy and Petrology* **160**, 683–704.
- Frost, D. J. (2006). The stability of hydrous mantle phases. In: Keppler, H. & Smyth, J. R. (eds) *Water in Nominally Anhydrous Minerals*. Mineralogical Society of America and Geochemical Society, *Reviews in Mineralogy and Geochemistry* **62**, 243–271.
- Garcia, M. O. (1996). Petrography and olivine and glass chemistry of lavas from the Hawaii Scientific Drilling Project. *Journal of Geophysical Research* **101**, 11701–11713.
- Garrido, C. J. & Bodinier, J. L. (1999). Diversity of mafic rocks in the Ronda peridotite: evidence for pervasive melt–rock reaction during heating of subcontinental lithosphere by upwelling asthenosphere. *Journal of Petrology* **40**, 729–754.
- Geldmacher, J. & Hoernle, K. (2000). The 72 Ma geochemical evolution of the Madeira hotspot (eastern North Atlantic): recycling of Paleozoic (9500 Ma) oceanic lithosphere. *Earth and Planetary Science Letters* **183**, 73–92.
- Gerlach, D., Leeman, W. & Avé Lallemand, H. G. (1981). Petrology and geochemistry of plagiogranite in the Canyon Mountain Ophiolite, Oregon. *Contributions to Mineralogy and Petrology* **77**, 82–92.
- Giret, A., Tourpin, S., Marc, S., Verdier, O. & Cottin, J.-Y. (2002). Volcanisme de l'île aux Pingouins, archipel Crozet, témoin de l'hétérogénéité du manteau fertile au sud de l'océan Indien. *Comptes Rendus Géosciences* **4**, 481–488.
- Gislason, S. R., Arnorsson, S. & Armannsson, H. (1996). Chemical weathering of basalt in Southwest Iceland; effects of runoff, age of rocks and vegetative/glacial cover. *American Journal of Science* **296**, 837–907.
- Gonzaga, R. G., Lowry, D., Jacob, D. E., LeRoex, A. P., Schulze, D. & Menzies, M. A. (2010). Eclogites and garnet pyroxenites: similarities and differences. *Journal of Volcanology and Geothermal Research* **190**, 235–247.
- Green, T. H. (1994). Experimental studies of trace-element partitioning applicable to igneous petrogenesis—Sedona 16 years later. *Chemical Geology* **117**, 1–36.
- Green, T. H., Blundy, J. D., Adam, J. & Yaxley, G. M. (2000). SIMS determination of trace element partition coefficients between garnet, clinopyroxene and hydrous basaltic liquids at 2–7.5 GPa and 1080–1200°C. *Lithos* **53**, 165–187.
- Gregoire, M., Moine, B. N., O'Reilly, S. Y., Cottin, J. Y. & Giret, A. (2000). Trace element residence and partitioning in mantle xenoliths metasomatized by highly alkaline, silicate- and carbonate-rich melts (Kerguelen Islands, Indian Ocean). *Journal of Petrology* **41**, 477–509.
- Grove, T. L., Holbig, E. S., Barr, J. A., Till, C. B. & Krawczynski, M. J. (2013). Melts of garnet lherzolite: experiments, models and comparison to melts of pyroxenite and carbonated lherzolite. *Contributions to Mineralogy and Petrology* **166**, 887–910.
- Gunn, B. M., Coy-Yil, R., Watkins, N. D., Abranson, C. E. & Nougier, J. (1970). Geochemistry of an oceanite–ankaramite–basalt suite from East Island, Crozet Archipelago. *Contributions to Mineralogy and Petrology* **28**, 319–339.
- Gurenko, A. A., Hoernle, K. A., Hauff, F., Schmincke, H.-U., Han, D., Miura, Y. N. & Kaneoka, I. (2006). Major, trace element and Nd–Sr–Pb–O–He–Ar isotope signatures of shield stage lavas from the central and western Canary Islands: insights into mantle and crustal processes. *Chemical Geology* **233**, 75–112.

- Gysi, A. P., Jagoutz, O., Schmidt, M. M. & Targuisti, K. (2011). Petrogenesis of pyroxenites and melt infiltrations in the ultramafic complex of Beni Bousera, Northern Morocco. *Journal of Petrology* **52**, 1–57.
- Halliday, A. N., Lee, D.-C., Tommasini, S., Davies, G. R., Paslick, C. R., Fitton, J. G. & James, D. E. (1995). Incompatible trace elements in OIB and MORB and source enrichment in the sub-oceanic mantle. *Earth and Planetary Science Letters* **133**, 379–395.
- Harlow, G. E. (1997). K in clinopyroxene at high pressure and temperature: an experimental study. *American Mineralogist* **82**, 259–269.
- Harris, C. & Bell, J. D. (1982). Natural partial melting of syenite blocks from Ascension Island. *Contributions to Mineralogy and Petrology* **79**, 107–113.
- Harris, R. N. & McNutt, M. K. (2007). Heat flow on hot spot swells: evidence for fluid flow. *Journal of Geophysical Research* **112**, B03407.
- Hartmann, G. & Wedepohl, K. H. (1993). The composition of peridotite tectonites from the Ivrea complex, northern Italy: residues from melt extraction. *Geochimica et Cosmochimica Acta* **57**, 1761–1782.
- Hawkesworth, C., Gallagher, K., Hergt, J. & McDermott, F. (1993). Trace element fractionation processes in the generation of Island Arc Basalts. *Philosophical Transactions of the Royal Society of London* **342**, 179–191.
- Hermann, J. & Spandler, C. J. (2008). Sediment melts at sub-arc depths: an experimental study. *Journal of Petrology* **49**, 717–740.
- Herzberg, C. & Asimow, P. D. (2008). Petrology of some oceanic island basalts: PRIMELT2.XLS software for primary magma calculation. *Geochemistry, Geophysics, Geosystems* **9**, Q09001.
- Herzberg, C. & Gazel, E. (2009). Petrological evidence for secular cooling in mantle plumes. *Nature* **458**, 619–623.
- Herzberg, C., Asimow, P. D., Arndt, N., Niu, Y., Leshner, C. M., Fitton, J. G., Cheadle, M. J. & Saunders, A. D. (2007). Temperatures in ambient mantle and plumes: constraints from basalts, picrites, and komatiites. *Geochemistry, Geophysics, Geosystems* **8**, Q02006.
- Hirschmann, M. (2000). Mantle solidus: experimental constraints and the effects of peridotite composition. *Geochemistry, Geophysics, Geosystems* **1**, doi:10.1029/2000GC000070.
- Hirschmann, M. M. & Stolper, E. M. (1996). A possible role for garnet pyroxenite in the origin of the 'garnet signature' in MORB. *Contributions to Mineralogy and Petrology* **124**, 185–208.
- Hoernle, K. & Schmincke, H. U. (1993). The petrology of the tholeiites through melilitite nephelinites on Gran Canaria, Canary Islands: crystal fractionation, accumulation and depths of melting. *Journal of Petrology* **34**, 573–597.
- Hoernle, K., Tilton, G., Le Bas, M. J., Duggen, S. & Garbeschönberg, D. (2002). Geochemistry of oceanic carbonatites compared with continental carbonatites: mantle recycling of oceanic crustal carbonate. *Contributions to Mineralogy and Petrology* **142**, 520–542.
- Hofmann, A. W. (1988). Chemical differentiation of the Earth: the relationship between mantle, continental crust and oceanic crust. *Earth and Planetary Science Letters* **90**, 297–314.
- Humphreys, E. R. & Niu, Y. (2009). On the composition of ocean island basalts (OIB): the effects of lithospheric thickness variation and mantle metasomatism. *Lithos* **112**, 118–136.
- Ito, G. & Mahoney, J. J. (2005a). Flow and melting of a heterogeneous mantle: 1. Method and importance to the geochemistry of ocean island and mid-ocean ridge basalts. *Earth and Planetary Science Letters* **230**, 29–46.
- Ito, G. & Mahoney, J. J. (2005b). Flow and melting of a heterogeneous mantle: 2. Implications for a chemically nonlayered mantle. *Earth and Planetary Science Letters* **230**, 47–63.
- Jacob, D. (2004). Nature and origin of eclogite xenoliths from kimberlites. *Lithos* **77**, 295–316.
- Jacob, D. E., Bizimis, M. & Salters, V. J. M. (2005). Lu–Hf and geochemical systematics of recycled ancient oceanic crust: evidence from Roberts Victor eclogites. *Contributions to Mineralogy and Petrology* **148**, 707–720.
- Jagoutz, E., Palme, H., Baddenhausen, H., Blum, K., Cendales, M. & Dreibus, G. (1979). The abundances of major, minor and trace elements in the Earth's mantle as derived from primitive ultramafic nodules. *Proceedings of the 10th Lunar and Planetary Science Conference. Geochimica et Cosmochimica Acta Supplement*, 2031–2050.
- Janney, P. E., Le Roex, A. P. & Carlson, R. W. (2005). Hafnium isotope and trace element constraints on the nature of mantle heterogeneity beneath the Central Southwest Indian Ridge (13°E to 47°E). *Journal of Petrology* **46**, 2427–2464.
- Johnson, M. C. & Plank, T. (1999). Dehydration and melting experiments constrain the fate of subducted sediments. *Geochemistry, Geophysics, Geosystems* **1**, doi:10.1029/1999GC000014.
- Kamenetsky, V. S., Eggins, S. M., Crawford, A. J., Green, D. H., Gasparon, M. & Falloon, T. J. (1998). Calcic melt inclusions in primitive olivine at 43°N MAR: evidence for melt–rock reaction melting involving clinopyroxene-rich lithologies during MORB generation. *Earth and Planetary Science Letters* **160**, 115–132.
- King, S. D. & Adam, C. (2014). Hotspot swells revisited. *Physics of the Earth and Planetary Interiors* **235**, 66–83.
- Klein, E., Langmuir, C. & Staudigel, H. (1991). Geochemistry of basalts from the Southeast Indian Ridge, 115°–138°E. *Journal of Geophysical Research* **96**, 2089–2107.
- Klein, E. M. & Langmuir, C. H. (1987). Global correlations of ocean ridge basalt chemistry with axial depth and crustal thickness. *Journal of Geophysical Research* **92**, 8089–8115.
- Klemme, S., Günther, D., Hametner, K., Prowatke, S. & Zack, T. (2006). The partitioning of trace elements between ilmenite, ulvöspinel, armalcolite and silicate melts with implications for the early differentiation of the moon. *Chemical Geology* **234**, 251–263.
- Koepke, J., Feig, S. T., Snow, J. & Freise, M. (2004). Petrogenesis of oceanic plagiogranites by partial melting of gabbros: an experimental study. *Contributions to Mineralogy and Petrology* **146**, 414–432.
- Konzett, J. & Ulmer, P. (1999). The stability of hydrous potassic phases in Iherzolitic mantle—an experimental study to 9.5 GPa in simplified and natural bulk compositions. *Journal of Petrology* **40**, 629–652.
- Kornprobst, J., Piboule, M., Roden, M. & Tabit, A. (1990). Corundum-bearing garnet clinopyroxenites at Beni Bousera (Morocco): original plagioclase-rich gabbros recrystallized at depth within the mantle? *Journal of Petrology* **31**, 717–745.
- Lameyre, J. & Nougier, J. (1982). Geology of Ile de l'Est, Crozet archipelago (TAAF). In: Craddock, C. (ed.) *Antarctic Geoscience*. Madison: University of Wisconsin Press, pp. 767–770.
- La Tourette, T., Hervig, R. L. & Holloway, J. R. (1995). Trace element partitioning between amphibole, phlogopite, and basanite melt. *Earth and Planetary Science Letters* **135**, 13–30.
- Le Bas, M. J., Le Maitre, R. W., Streckeisen, A. & Zanettin, B. (1986). A chemical classification of volcanic rocks based on the total alkali–silica diagram. *Journal of Petrology* **27**, 745–750.

- Le Roex, A. P., Bell, D. R. & Davis, P. (2003). Petrogenesis of Group I kimberlites from Kimberley, South Africa: evidence from bulk-rock geochemistry. *Journal of Petrology* **44**, 2261–2286.
- Longpré, M.-A., Troll, V. R. & Hansteen, T. H. (2008). Upper mantle magma storage and transport under a Canarian shield-volcano, Teno, Tenerife (Spain). *Journal of Geophysical Research* **113**, doi:10.1029/2007JB005422.
- Luth, R. W. (1997). Experimental study of the system phlogopite–diopside from 3.5 to 17 GPa. *American Mineralogist* **82**, 1198–1210.
- Lyubetskaya, T. & Korenaga, J. (2007). Chemical composition of Earth's primitive mantle and its variance: 1. Method and results. *Journal of Geophysical Research* **112**, B03211.
- Macdonald, G. A. (1968). Composition and origin of Hawaiian lavas. *Geological Society of America Bulletin* **116**, 477–521.
- Mahoney, J. J., White, W. M., Upton, B. G. J., Neal, C. R. & Scrutton, R. A. (1996). Beyond EM-1: lavas from Afanasy–Nikitin Rise and the Crozet archipelago, Indian Ocean. *Geology* **24**, 615–618.
- Manglik, A. & Christensen, U. R. (1997). Effect of mantle depletion buoyancy on plume flow and melting beneath a stationary plate. *Journal of Geophysical Research* **102**, 5019–5028.
- Maria, A. H. & Luhr, J. F. (2008). Lamprophyres, basanites, and basalts of the Western Mexican Volcanic Belt: volatile contents and a vein–wallrock melting relationship. *Journal of Petrology* **49**, 2123–2156.
- McDade, P., Wood, B. & Blundy, J. (2003). Near solidus trace element partitioning between Tinaquillo lherzolite and melt at 1.5 GPa. *Physics of the Earth and Planetary Interiors* **139**, 129–147.
- McDonough, W. F. & Sun, S.-S. (1995). Composition of the Earth. *Chemical Geology* **120**, 223–253.
- McKenzie, D. (1989). Some remarks on the movement of small melt fractions in the mantle. *Earth and Planetary Science Letters* **95**, 53–72.
- Mengel, K. & Green, D. H. (1989). Stability of amphibole and phlogopite in metasomatized peridotite under water-saturated and water-undersaturated conditions. In: Ross, J. (ed.) *Kimberlites and Related Rocks: their Occurrence, Origin and Emplacement*. Geological Society of Australia, Special Publication **14**, 571–581.
- Meyzen, C. M., Toplis, M. J., Humler, E., Ludden, J. & Mevel, C. (2003). A discontinuity in mantle composition beneath the southwest Indian ridge. *Nature* **421**, 731–733.
- Meyzen, C. M., Massironi, M., Pozzobon, R. & Dal Zilio, L. (2015). Are terrestrial plumes from motionless plates analogues to Martian plumes feeding the giant shield volcanoes? In: Platz, T., Massironi, M., Byrne, P. K. & Hiesinger, H. (eds) *Volcanism and Tectonism Across the Inner Solar System*. Geological Society, London, Special Publications **401**, 107–126.
- Monnereau, M. & Cazenave, A. (1990). Depth and geoid anomalies over oceanic hotspot swells: A global survey. *Journal of Geophysical Research* **95**, 15429–15438.
- Montelli, R., Nolet, G., Dahlen, F. A., Masters, G., Engdahl, E. R. & Hung, S.-H. (2004). Finite-frequency tomography reveals a variety of plumes in the mantle. *Science* **303**, 338–343.
- Montelli, R., Nolet, G., Dahlen, F. A. & Masters, G. (2006). A catalogue of deep mantle plumes: new results from finite frequency tomography. *Geochemistry, Geophysics, Geosystems* **7**, Q11007.
- Müller, R. D., Sdrolias, M., Gaina, C. & Roest, W. R. (2008). Age, spreading rates, and spreading asymmetry of the world's ocean crust. *Geochemistry, Geophysics, Geosystems* **9**, Q04006.
- Newsom, H. E., White, W. M., Jochum, K. P. & Hofmann, A. W. (1986). Siderophile and chalcophile element abundances in oceanic basalts, lead isotope evolution and growth of the Earth's core. *Earth and Planetary Science Letters* **80**, 299–313.
- Niida, K. & Green, D. H. (1999). Stability and chemical composition of pargasitic amphibole in MORB pyrolite under upper mantle conditions. *Contributions to Mineralogy and Petrology* **135**, 18–40.
- Niu, Y., Waggoner, D. G., Sinton, J. M. & Mahoney, J. J. (1996). Mantle source heterogeneity and melting processes beneath seafloor spreading centers: the East Pacific Rise, 18°–19°S. *Journal of Geophysical Research* **101**, 27711–27733.
- Niu, Y., Wilson, M., Humphreys, E. R. & O'Hara, M. J. (2011). The origin of intra-plate ocean island basalts (OIB): the lid effect and its geodynamic implications. *Journal of Petrology* **52**, 1443–1468.
- O'Reilly, S. Y. & Griffin, W. L. (2013). Mantle metasomatism. In: Harlow, D. E. & Austrheim, H. (eds) *Metasomatism and the Chemical Transformation of Rock: the Role of Fluids in Terrestrial and Extraterrestrial Processes*. New York: Springer, pp. 471–534.
- Palme, H. & O'Neill, H. S. C. (2004). Cosmochemical estimates of mantle composition. In: Carlson, R. W., Holland, H. D. & Turekian, K. K. (eds) *Treatise on Geochemistry, Vol. 2. The Mantle and Core*. Amsterdam: Elsevier, pp. 1–38.
- Parman, S. W. & Grove, T. L. (2004). Harzburgite melting with and without H₂O: Experimental data and predictive modeling. *Journal of Geophysical Research* **109**, doi:10.1029/2003JB002566.
- Parsons, B. & Sclater, J. G. (1977). An analysis of the variation of ocean floor bathymetry and heat flow with age. *Journal of Geophysical Research* **82**, 803–827.
- Paul, D., Kamenetsky, V. S., Hofmann, A. W. & Stracke, A. (2007). Compositional diversity among primitive lavas of Mauritius, Indian Ocean: Implications for mantle sources. *Journal of Volcanology and Geothermal Research* **164**, 76–94.
- Pearson, D. G., Davies, G. R. & Nixon, P. H. (1993). Geochemical constraints on the petrogenesis of diamond facies pyroxenites from the Beni Bousera peridotite massif, North Morocco. *Journal of Petrology* **34**, 125–172.
- Pedersen, R. & Malpas, J. (1984). The origin of oceanic plagiogranites from the Karmøy ophiolite, western Norway. *Contributions to Mineralogy and Petrology* **88**, 36–52.
- Phipps Morgan, J. & Smith, W. H. F. (1992). Flattening of the seafloor depth–age curve as a response to asthenospheric flow. *Nature* **359**, 524–527.
- Phipps Morgan, J., Morgan, W. J. & Price, E. (1995). Hotspot melting generates both hotspot volcanism and a hotspot swell? *Journal of Geophysical Research: Solid Earth* **100**, 8045–8062.
- Prägel, N.-O. & Holm, P. M. (2006). Lithospheric contributions to high-MgO basanites from the Cumbre Vieja Volcano, La Palma, Canary Islands and evidence for temporal variation in plume influence. *Journal of Volcanology and Geothermal Research* **149**, 213–239.
- Prowatke, S. & Klemme, S. (2006). Trace element partitioning between apatite and silicate melts. *Geochimica et Cosmochimica Acta* **70**, 4513–4527.
- Putirka, K. (1999). Melting depths and mantle heterogeneity beneath Hawaii and the East Pacific Rise: constraints from Na/Ti and rare earth element ratios. *Journal of Geophysical Research* **104**(B2), 2817–2829.
- Putirka, K. (2005). Mantle potential temperatures at Hawaii, Iceland, and the mid-ocean ridge system, as inferred from

- olivine phenocrysts: evidence for thermally driven mantle plumes. *Geochemistry, Geophysics, Geosystems* **6**, Q05L08.
- Putirka, K. (2008). Excess temperatures at ocean islands: implications for mantle layering and convection. *Geology* **36**, 283–286.
- Putirka, K., Johnson, M., Kinzler, R. J., Longhi, J. & Walker, D. (1996). Thermobarometry of mafic igneous rocks based on clinopyroxene–liquid equilibria, 30 kbar. *Contributions to Mineralogy and Petrology* **123**, 92–108.
- Recq, M., Goslin, J., Charvis, P. & Operto, S. (1998). Small-scale crustal variability within an intraplate structure: the Crozet bank (southern Indian Ocean). *Geophysical Journal International* **134**, 145–156.
- Reiners, P. W. & Nelson, B. K. (1998). Temporal–compositional–isotopic trends in rejuvenated-stage magmas of Kauai, Hawaii, and implications for mantle melting processes. *Geochimica et Cosmochimica Acta* **62**, 2347–2368.
- Robinson, J. A. C. & Wood, B. J. (1998). The depth of the spinel to garnet transition at the peridotite solidus. *Earth and Planetary Science Letters* **164**, 277–284.
- Rogers, N. W., Hawkesworth, C. J. & Palacz, Z. A. (1992). Phlogopite in the generation of olivine–mellilitites from Namaqualand, South Africa and implications for element fractionation processes in the upper mantle. *Lithos* **28**, 347–365.
- Rohde, J., Hoernle, K., Hauff, F., Werner, R., Connor, J. O., Class, C., Garbe-Schönberg, D. & Jokat, W. (2013). 70 Ma chemical zonation of the Tristan–Gough hotspot track. *Geology*. doi:10.1130/G33790.33791.
- Safonov, O. G., Bindi, L. & Vinograd, V. L. (2011). Potassium-bearing clinopyroxene: a review of experimental, crystal chemical and thermodynamic data with petrological applications. *Mineralogical Magazine* **75**, 2467–2484.
- Salters, V. & Longhi, J. (1999). Trace element partitioning during the initial stages of melting beneath mid-ocean ridges. *Earth and Planetary Science Letters* **166**, 15–30.
- Salters, V., Longhi, J. E. & Bizimis, M. (2002). Near mantle solidus trace element partitioning at pressures up to 3.4 GPa. *Geochemistry, Geophysics, Geosystems* **3**, doi:10.1029/2001GC000148.
- Sandwell, D. T. & McAdoo, D. C. (1990). High-accuracy, high-resolution gravity profiles from 2 years of the Geosat Exact Repeat Mission. *Journal of Geophysical Research: Oceans* **95**, 3049–3060.
- Scambelluri, M., Hermann, J., Morten, L. & Rampone, E. (2006). Melt-versus fluid-induced metasomatism in spinel to garnet wedge peridotites (Ulten Zone, Eastern Italian Alps): clues from trace element and Li abundances. *Contributions to Mineralogy and Petrology* **151**, 372–394.
- Schmidt, K., Bottazzi, P., Vannucci, R., Mengel, K. & Abouchami, W. (1999). Trace element partitioning between phlogopite, clinopyroxene and leucite lamproite melt. *Earth and Planetary Science Letters* **168**, 287–299.
- Schmidt, M., Vielzeuf, D. & Auzanneau, E. (2004). Melting and dissolution of subducting crust at high pressures: the key role of white mica. *Earth and Planetary Science Letters* **228**, 65–84.
- Schutt, D. L. & Leshner, C. E. (2006). Effects of melt depletion on the density and seismic velocity of garnet and spinel lherzolite. *Journal of Geophysical Research* **111**, B05401.
- Schwarz, S., Klugel, A. & Wohlgemuth-Ueberwasser, C. (2004). Melt extraction pathways and stagnation depths beneath the Madeira and Desertas rift zones (NE Atlantic) inferred from barometric studies. *Contributions to Mineralogy and Petrology* **147**, 228–240.
- Segard, M., Bezos, A. & La, C. (2011). Petrology and geochemistry of Crozet hotspot alkali basalts: evaluation of the source mineralogy. Abstract V51E-2559 presented at 2011 Fall Meeting, San Francisco AGU, San Francisco, CA, 5–9 December.
- Shorttle, O., Maclennan, J. & Lambart, S. (2014). Quantifying lithological variability in the mantle. *Earth and Planetary Science Letters* **395**, 24–40.
- Sisson, T. W., Kimura, J.-I. & Coombs, M. L. (2009). Basanite–nephelinite suite from early Kilauea: carbonated melts of phlogopite–garnet peridotite at Hawaii’s leading magmatic edge. *Contributions to Mineralogy and Petrology* **158**, 803–829.
- Sleep, N. H. (1990). Hotspots and mantle plumes: some phenomenology. *Journal of Geophysical Research* **95**, 6715–6736.
- Sobolev, A. V., Hofmann, A. W., Sobolev, S. V. & Nikogosian, I. K. (2005). An olivine-free mantle source of Hawaiian shield basalts. *Nature* **341**, 1–8.
- Stein, C. A. (1995). Heat flow of the Earth. In: Ahrens, T. J. (ed.) *Global Earth Physics: A Handbook of Physical Constants*. Washington, DC: American Geophysical Union, pp. 144–158.
- Stein, C. A. & Stein, S. (1992). A model for the global variation in oceanic depth and heat flow with lithospheric age. *Nature* **359**, 123–129.
- Sun, S.-S. & McDonough, W. (1989). Chemical and isotopic systematics of oceanic basalts: implications for mantle composition and processes. In: Saunders, A. D. & Norry, M. J. (eds) *Magmatism in the Ocean Basins*. Geological Society, London, Special Publications **42**, 313–345.
- Taylor, S. R. & McLennan, M. (1985). *The Continental Crust: its Composition and Evolution*. Oxford: Blackwell Scientific.
- Thibault, Y., Edgar, A. D. & Lloyd, F. E. (1992). Experimental investigation of melts from a carbonated phlogopite lherzolite: implications for metasomatism in the continental lithospheric mantle. *American Mineralogist* **77**, 784–794.
- Tiepolo, M., Vannucci, R., Bottazzi, P., Oberti, R., Zanetti, A. & Foley, S. (2000). Partitioning of rare earth elements, Y, Th, U, and Pb between pargasite, kaersutite, and basanite to trachyte melts: implications for percolated and veined mantle. *Geochemistry, Geophysics, Geosystems* **1**, doi:10.1029/2000GC000064.
- Tiepolo, M., Oberti, R. & Zanetti, A. (2007). Trace-element partitioning between amphibole and silicate melt. In: Hawthorne, F. C., Oberti, R., Della Ventura, G. & Mottana, A. (eds) *Amphiboles: Crystal Chemistry, Occurrence, and Health Issues*. Reviews in Mineralogy & Geochemistry. Mineralogical Society of America and Geochemical Society, Reviews in Mineralogy **67**, 417–452.
- Tsuruta, K. & Takahashi, E. (1998). Melting study of an alkali basalt JB-1 up to 12.5 GPa: behavior of potassium in the deep mantle. *Physics of the Earth and Planetary Interiors* **107**, 119–130.
- Tuff, J. & Gibson, S. A. (2007). Trace-element partitioning between garnet, clinopyroxene and Fe-rich picritic melts at 3 to 7 GPa. *Contributions to Mineralogy and Petrology* **153**, 369–387.
- Van Achtenbergh, E., Griffin, W. L. & Stiefenhofer, J. (2001). Metasomatism in mantle xenoliths from the Lethakane kimberlites: estimation of element fluxes. *Contributions to Mineralogy and Petrology* **141**, 397–414.
- Van Der Zander, I., Sinton, J. M. & Mahoney, J. J. (2010). Late shield-stage silicic magmatism at Wai’anae volcano: Evidence for hydrous crustal melting in Hawaiian volcanoes. *Journal of Petrology* **51**, 671–701.
- Van Westrenen, W., Blundy, J. & Wood, B. (1999). Crystal-chemical controls on trace element partitioning between

- garnet and anhydrous silicate melt. *American Mineralogist* **84**, 838–847.
- Verwoerd, W., Chevallier, L., Thomson, J. W., Nougier, J., Barling, J., Tingey, R. J., Wright, A. C., Kyle, P. R. & Rowley, P. D. (1990). Oceanic islands on the Antarctic Plate. In: Baker, P., Kyle, P., Rowley, P. D., Smellie, J. & Verwoerd, W. (eds) *Volcanoes of the Antarctic Plate and Southern Oceans*. Washington: American Geophysical Union, pp. 396–463.
- Wallace, M. E. & Green, D. H. (1988). An experimental determination of primary carbonatite magma composition. *Nature* **333**, 343–346.
- Walter, M. J. (1998). Melting of garnet peridotite and the origin of komatiite and depleted lithosphere. *Journal of Petrology* **39**, 29–60.
- Wendlandt, R. F. & Eggler, D. H. (1980). The origins of potassic magmas: 2. Stability of phlogopite in natural spinel lherzolite and in the system $\text{KAlSiO}_4\text{-MgO-SiO}_2\text{-H}_2\text{O-CO}_2$ at high pressures and high temperatures. *American Journal of Science* **280**, 421–458.
- Willbold, M. & Stracke, A. (2006). Trace element composition of mantle end-members: implications for recycling of oceanic and upper and lower continental crust. *Geochemistry, Geophysics, Geosystems* **7**, Q04004.
- Williams, H. & Bizimis, M. (2014). Iron isotope tracing of mantle heterogeneity within the source regions of oceanic basalts. *Earth and Planetary Science Letters* **404**, 396–407.
- Wolff, P. E., Koepke, J. & Feig, S. T. (2013). The reaction mechanism of fluid-induced partial melting of gabbro in the oceanic crust. *European Journal of Mineralogy* **25**, 279–298.
- Wood, B. J. & Blundy, J. D. (1997). A predictive model for rare earth element partitioning between clinopyroxene and anhydrous silicate melt. *Contributions to Mineralogy and Petrology* **129**, 166–181.
- Woodhead, J. D. (1996). Extreme HIMU in an oceanic setting: the geochemistry of Mangaia Island (Polynesia), and temporal evolution of the Cook–Austral hotspot. *Journal of Volcanology and Geothermal Research* **72**, 1–19.
- Wulff-Pedersen, E., Neumann, E.-R. & Jensen, B. B. (1996). The upper mantle under La Palma, Canary Islands: formation of Si–K–Na-rich melt and its importance as a metasomatic agent. *Contributions to Mineralogy and Petrology* **125**, 113–139.
- Yoshikawa, M., Nakamura, E. & Takahashi, N. (1993). Rb–Sr isotope systematics in a phlogopite-bearing spinel lherzolite and its implications for age and origin of metasomatism in the Horoman peridotite complex, Hokkaido, Japan. *Journal of Mineralogy, Petrology and Economic Geology* **88**, 121–130.
- Zanetti, A., Mazzucchelli, M., Rivalenti, G. & Vannucci, R. (1999). The Finero phlogopite-peridotite massif: an example of subduction-related metasomatism. *Contributions to Mineralogy and Petrology* **134**, 107–122.
- Zanetti, A., Mazzucchelli, M., Sinigoi, S., Giovanard, T., Peressini, G. & Fanning, M. (2013). SHRIMP U–Pb zircon Triassic intrusion age of the Finero mafic complex (Ivrea–Verbano Zone, Western Alps) and its geodynamic implications. *Journal of Petrology* **54**, 2235–2265.
- Zhou, X. (1996). Île de l’Est (Crozet archipelago, Southwestern Indian Ocean): petrogenesis of the plutonic complexes. Ph.D. Thesis, Université Libre de Bruxelles, 214 pp.